OFF-periods reduce the complexity of neocortical activity during sleep

Joaquín González[1], Matias Cavelli[1,2], Adriano BL Tort[3], Pablo Torterolo[1], and Nicolás Rubido[4,5,*]

[1]Universidad de la República, Departamento de Fisiología, Facultad de Medicina, Av. Gral. Flores 2125, 11800 Montevideo, Uruguay.
[2]Department of Psychiatry, University of Wisconsin, Madison, WI, 53558, USA.
[3]Brain Institute, Federal University of Rio Grande do Norte, Natal, RN 59056, Brazil
[4]University of Aberdeen, Aberdeen Biomedical Imaging Centre, Aberdeen AB25 2ZG, United Kingdom.
[5]Universidad de la República, Instituto de Física de Facultad de Ciencias, Iguá 4225, 11400 Montevideo, Uruguay. *nrubido@fisica.edu.uy

Abstract

Field recordings decrease their temporal complexity during slow-wave sleep (SWS), however, the neural mechanism for this decrease remains elusive. Here, we show that this complexity reduction is caused by synchronous neuronal OFF-periods by analysing in-vivo recordings from neocortical neuronal populations. We find that OFF-periods trap cortical dynamics, disrupting causal interactions and making the population activity more recurrent, deterministic, and less chaotic than during REM sleep or Wakefulness. Moreover, when we exclude OFF-periods, SWS becomes indistinguishable from Wakefulness or REM sleep. In fact, for all states, we show that the spiking activity has a universal scaling compatible with critical phenomena. We complement these results by analysing a critical branching model that replicates the experimental findings, where we show that forcing OFF-periods into a percentage of neurons suffices to generate a decrease in complexity that replicates SWS.

Introduction

The loss of temporal complexity is characteristic of unconsciousness – including deep sleep states – and can be widely observed in field recordings, such as electroencephalograms (EEG) [1–14]. Complexity can be defined as the diversity of patterns in a given signal, which approximately quantifies its information content. High complexity is observed from field recordings during Wakefulness, decreasing as awareness is lost [1,2,4–6,8,13,14], which suggests that consciousness needs a complex substrate [15,16]. Moreover, these complexity changes are conserved across species (such as mice [17], rats [10,11], monkeys [13], and humans [3, 6, 8, 12]) and are influenced by circadian rhythms [18], age [19], and pathology [9, 20], pointing to the existence of a fundamental state of cortical circuits during the sleep-wake cycle.

In the last decade, there has been a significant rise in the use of complexity measures to analyse field recordings [1–9, 9–14, 17–20] (Fig.S1). Mainly, because these are efficient measures to reveal underlying non-linear effects. In spite of the use of these measures, we still lack a complete understanding of the neural-substrate that causes the loss of temporal complexity [21]. In particular, to get the neural substrate from an EEG, we need to deconstruct the field recording to a set of neural sources (e.g., a set accounting for their spiking activity). However, for any given EEG recording, there are infinite ways to combine neural sources that can be used to recreate it, which is known as the inverse problem [22]. Moreover, the contribution of extra-neural sources to the field measurements creates another problem [23]. For example, muscular noise contamination and movement artefacts decrease during sleep [10], potentially confounding the changes reported in the EEG complexity.

In contrast, *in-vitro* studies have shown that complex patterns of spiking activity characterise isolated neuronal populations [24, 25]. Furthermore, slow waves are able to reduce the complexity of these recordings [27]. During natural slow-wave sleep (SWS), neuronal activity synchronises in periods of quiescence, known as OFF-periods, associated with the slow oscillation [29–31]. As these periods hinder neural interactions [28], they would be expected to affect cortical dynamics. For example, a sleep-like OFF-period activity disrupted complexity in patients with unresponsive wakefulness syndrome [26]. This suggests a possible link between the loss of temporal complexity during sleep and the occurrence of slow waves and OFF-periods. Nevertheless, to the best of our knowledge, we still lack a sound justification to claim that (1) the loss of complexity observed in field recordings during sleep is of neural origin (instead of artefactual) and (2) is caused by the presence of synchronous OFF-periods.

In this work, we analyse groups of individual neurons *in-vivo* – hereafter referred as population activity – during the natural sleep-wake cycle, aiming to understand the origin of the complexity changes in field recordings and the effects of the slow waves during sleep. We note that estimating the field activity from unitary recordings is a well poised forward-problem (unlike the inverse problem), allowing us to make inferences about the origin of complexity changes in field recordings. Our results show that the population activity, in the neocortex and hippocampus, is less complex during SWS because their evolution gets periodically trapped. These trapped states correspond to the population OFF-periods, which involve almost all neurons recorded in a single area and cause the field recordings to reduce their complexity. In addition, the activity during SWS outside the OFF-periods is indistinguishable to that of Wakefulness or REM, and follows an universal scaling similar to those found in critical phenomena. We confirm this observation by modelling the cortex as a critical branching process, which besides reproducing our *in-vivo* results, it shows how the cortex balances complex patterns and synchronised inactivity (OFF-periods). Overall, our results indicate that the decrease in complexity is a sleep trait stemming from the cortex neural substrate caused by the inclusion of synchronous OFF-periods in a near-critical system.

Results

In this work, we study *in-vivo* recordings from $\simeq$ 1600 neurons registered in 31 sessions (each session measures 51 $\pm$ 5 neurons from a given cortical area; details in Datasets within the Sect. Methods) for 15 rats in freely moving conditions, cycling through the states of sleep and wakefulness. In what follows, we present results from applying Recurrence Quantification Analysis (RQA) [32] to the population activity during the states of wakefulness (Wake), slow-wave sleep (SWS), and rapid-eye movement (REM) sleep, which explain the complexity changes observed from field recordings in various works [2, 3, 8–12, 14].

Recurrence analysis reduces high-dimensional dynamics to a 2D representation

Population activity defines a high-dimensional phase-space, where neuronal ensembles evolve in trajectories conforming attractors. Through the sleep-wake states, the ensemble's attractor changes. Specifically, the spiking activity from the recorded neuronal ensembles (i.e., the data-sets) detail the system's instantaneous state at any given time and for any sleep-wake state (Fig. 1**A**). The system's evolution is then given by a trajectory, which accounts for the firing counts as they evolve in this phase-space (Fig. 1**B**). An attractor is then evidenced as a manifold that attracts different trajectories of the system to the same region of phase-space – the more convoluted (fractal) the attractor is, the higher the temporal complexity of its trajectories. However, the attractor resulting from the recordings of any given cortical area is typically high-dimensional; note that 50 neurons hold a $\sim 50D$ phase-space. Consequently, by applying RQA we reduce the dimensions to the analysis of $2D$ recurrence plots (Fig. 1**C**).

In this work, recurrence plots are constructed as follows. Let a trajectory be $\{\vec{x}(t_1), \vec{x}(t_2), \ldots, \vec{x}(t_n)\}$, where $\vec{x}(t_i)$ is the vector containing the firing counts, $x_k(t_i)$, for each neuron in the ensemble ($k = 1, \ldots, N$), at time, t_i, with $i = 1, \ldots, T$, T being the length of the recording (we choose, $T = 10\ s$). The firing counts for each neuron, x_k, are found from integrating the spike trains within 50 *ms* time-bins; namely, $t_{i+1} - t_i = 50\ ms\ \forall\, i$. This choice comes from the physiological definition of an OFF-period, i.e., a period $\geq$ 50 *ms* without spikes. As a result, the firing-variable is an integer that can take values from 0 up to 50 (assuming a maximum of 1 spike per *ms*). A recurrence plot is then defined by a symmetric matrix, R, whose entries are: $R(i, j) = 1$ if

$\left\|\vec{x}(t_i) - \vec{x}(t_j)\right\| < \epsilon$, or $R(i,j) = 0$ otherwise, with $i, j = 1, \ldots, T$. Therefore, a recurrence happens whenever the system's trajectory returns to the same region of phase space up to ϵ, where $\epsilon > 0$ sets the tolerance level for defining closeness. Here, we set $\epsilon = \sigma_p$, where σ_p is the standard deviation for the population activity being analysed (during wakefulness), namely, the cortical-area's standard deviation. This tolerance guarantees a sufficiently sparse recurrence-plot, but still with sufficient points to carry the statistical analyses. In fact, all our results are robust, being invariant to changes in ϵ or the bin size (Fig. S2).

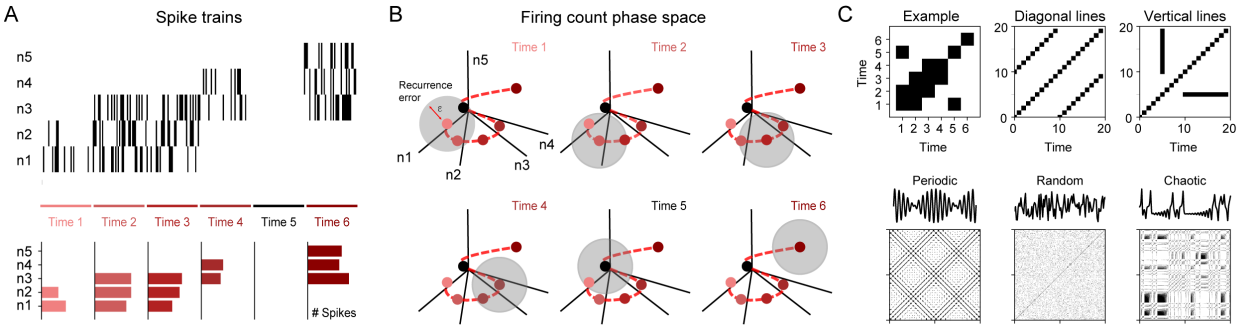

Figure 1: Recurrence example of population activity. **A** Example of spike trains for 5 neurons. Their firing rates are shown in the bottom panel for the respective time-bins, where an OFF-period can be seen at time 5. **B** Resultant phase-space trajectory (evolution), where each axis is the firing rate of a neuron. The system's trajectory is shown by the dashed line and its (binned) measurements by the filled circles. For each measurement, a ball of radius ϵ (shaded grey area) is used to find when the trajectory recurs to the same region, defining a recurrence plot (RP). **C** (Top left panel) RP for the trajectory from **B**. (Remaining panels) RP examples, showing diagonal lines, vertical lines, as well as periodic, random, and chaotic trajectories.

Two types of general structures appear in a recurrence plot: diagonal lines, which originate from periodic trajectories, and vertical lines, which originate by trapped or frozen trajectories. These structures serve to differentiate between periodic, random, or chaotic trajectories (see corresponding panels in Fig. 1**C**), which are then quantified by different metrics (see RQA in Methods). In particular, we measure (i) Recurrence Rates (density of points in a recurrence plot), RR, (ii) Determinism (proportion of points forming diagonal lines), DET, (iii) Laminarity (proportion of points forming vertical lines), LAM, (iv) Trapping Times (the average length of the vertical lines), TT, and (v) Divergences (inverse of the longest diagonal line), DIV. RR quantifies the overall recurrence of the system, DET measures the smoothness of trajectories, LAM quantifies the proportion of recurrences caused by trapped states, TT measures the average time the system spends trapped in one of these states, and DIV quantifies the chaoticity in the system's evolution. Thus, the predictability of the system's trajectory is quantified by RR, DET, LAM, and TT, where the larger [smaller] their values the more [less] predictable. On the other hand, the system's chaoticity is mainly quantified by DIV, where the larger [smaller] its value the more [less] chaotic.

Neuronal activity decreases its complexity during slow-wave sleep

Here, we analyse data from the frontal cortex ($\sim$ 900 neurons), where we quantify the recurrence plots for Wake, SWS, and REM states. Fig 2**A** shows a representative local field potential (LFP) and spike trains for each frontal-cortex neuron (Neuron #). The corresponding recurrence plots for these examples are shown in Fig. 2**B**, which are constructed from 10 *s* windows of the firings counts within 50 *ms* bins (i.e., accumulated spike-trains). From these panels, we note that SWS exhibits denser recurrence plots than Wake or REM sleep; namely, SWS has firing patterns that recur more often than Wake or REM sleep. Also, SWS shows a distinctive square-shaped recurrence pattern lasting approximately 100 *ms*. This characteristic square-shape indicates that the frontal-cortex activity during SWS is partly periodic with trappings into frozen states, making it qualitatively less complex than Wake or REM sleep.

RQA confirms that during SWS the frontal-cortex activity is significantly more predictable and less chaotic than during Wake or REM sleep (i.e., less complex), as it can be seen from the box-plots in Fig. 2**C**. Statistics are shown in table S1. SWS has the highest average RR, DET, LAM and TT, indicating a higher

predictability for the neuronal activity during SWS than during Wake or REM sleep. On the contrary, DIV is larger during Wake and REM sleep than during SWS, indicating that SWS is significantly less chaotic.

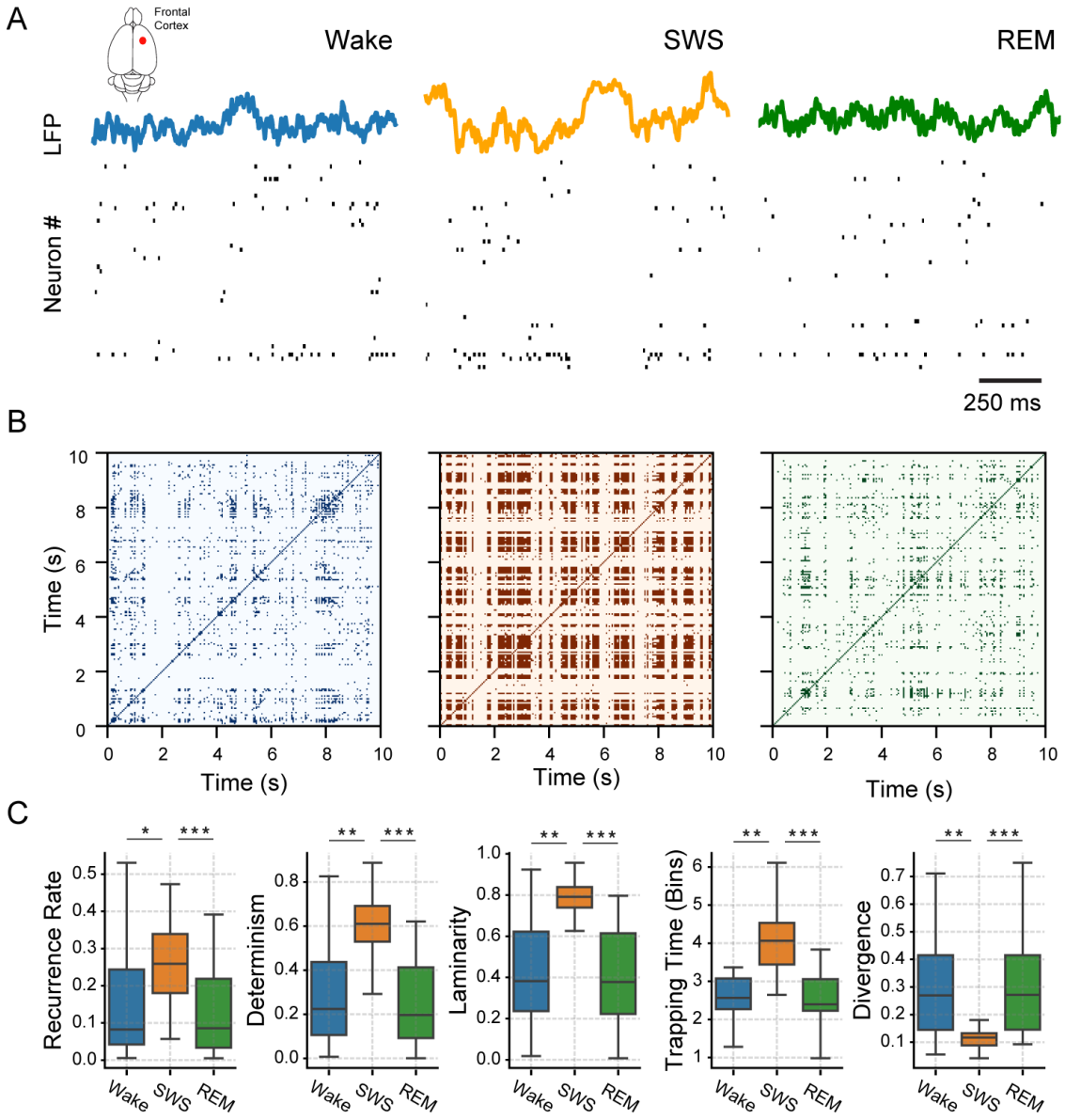

Figure 2: Recurrence analysis of in-vivo population activity from the frontal cortex. **A** Local field potentials (top trace) and spike-trains raster plots (1 *s* interval) for a representative rat during Wake (left panel), SWS (middle panel), and REM sleep (right panel). **B** Respective recurrence plots constructed from a 10 *s* interval of the population activity after binning the spike trains into 50 *ms* windows. **C** Recurrence Quantification Analysis for the sleep-wake states in **A** and **B** panels using 5 RQA metrics (titles in panels). For each metric, box-plots are constructed from the results of 12 animals and 24 sessions (outliers are not shown).$* = P < 0.001$, $** = P < 0.0001$, $*** = P < 0.00001$ (corrected by multiple comparisons).

These results show that during SWS, firing activity from the frontal cortex becomes (quasi-)periodically trapped in frozen trajectories, reducing the trajectory's complexity. On the contrary, Wake and REM sleep states show similar unpredictability and chaoticity for their ensemble firings, which indicate a higher complexity. Altogether, these firing patterns explain the reduction in temporal complexity during sleep that has been reported in field recordings [2, 3, 5, 8–12, 14]. Moreover, we find that these results hold when we

divide the frontal-cortex data into specific areas, as well as when we compare them to population activity registered from the hippocampus (Fig. 3); demonstrating the robustness in our conclusions.

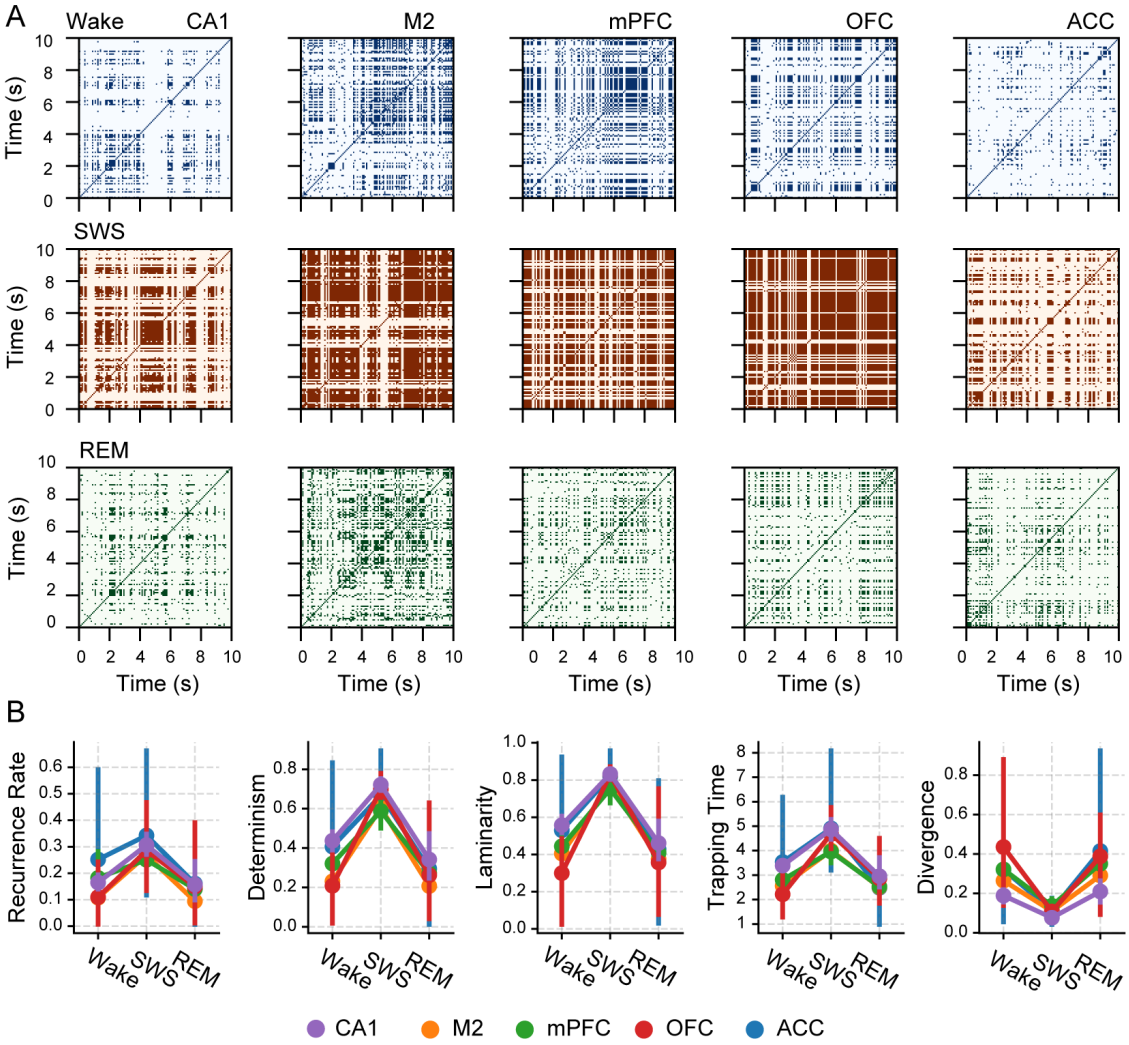

Figure 3: Recurrence analysis for different cortical locations. A Examples of recurrence plots for 10 *s* windows of the binned spike-trains (50 *ms* bins) for different locations during Wake, SWS, and REM sleep. Panels in each column correspond to the Hippocampus (CA1), secondary motor-cortex (M2), medial pre-frontal cortex (mPFC), orbito-frontal cortex (OFC), and the anterior cingulate cortex (ACC). **B** RQA metrics for all cortical locations in each sleep-wake state, where filled circles are the population averages and error bars show the corresponding 95 % confidence interval. $* = P < 0.05$, $** = P < 0.01$, $*** = P < 0.001$

Specifically, we select data from the secondary motor-cortex (M2), medial pre-frontal cortex (mPFC), orbito-frontal cortex (OFC), and the anterior cingulate cortex (ACC). Moreover, we include data from the hippocampus CA1 region. For these selections, our analysis shows consistently that neuronal spiking-activity decreases its temporal complexity during SWS (Fig. 3). Statistics for CA1 are shown in table S2.

For each cortex, Fig. 3**A** is composed of recurrence-plot examples for each sleep-wake state and Fig. 3**B** shows the RQA metrics for all cortical locations and their comparative statistics. We can see that all regions – hippocampus and neocortex – show differences across states. Particularly, from Fig. 3**A** we can see that irrespective of the region, Wake and REM have more complex recurrence-patterns than SWS, which again show trapped regions. From applying RQA to the hippocampus, we find that SWS has the highest RR, DET, LAM, and TT; similarly to the frontal cortex results (Fig. 2). Also, the DIV is larger during Wake or REM than during SWS. In addition, we find no significant differences when we compare the RQA across cortical

locations, RR (P = 0.68), DET (P = 0.39), LAM (P = 0.69), TT (P = 0.21) and DIV (P = 0.46). Therefore, we conclude that the decrease in complexity during SWS is a global feature of the population activity.

OFF-periods explain the complexity changes during SWS in the neocortex

RQA shows that complexity reduction during SWS is mainly due to the presence of frozen trajectories, which are the square-like patterns appearing in the recurrence plots. Hence, we study whether the existence of frozen trajectories correlates with the well-known neocortical OFF-periods [29–31], which are characterised as $\sim 85\,ms$-long periods where almost all neurons remain silent [29]; an example is shown in Fig. 4**A**. The importance of this study comes from the fact that the EEG reflects the synchronous activity of pyramidal neocortical neurons [33], where OFF-periods are evidenced by the presence of slow EEG oscillations ($0-4\,Hz$) [29, 30, 34]. Therefore, the correlation between frozen trajectories and OFF-periods (Fig. 4**B**) can provide a physiological mechanism for the loss of complexity during sleep.

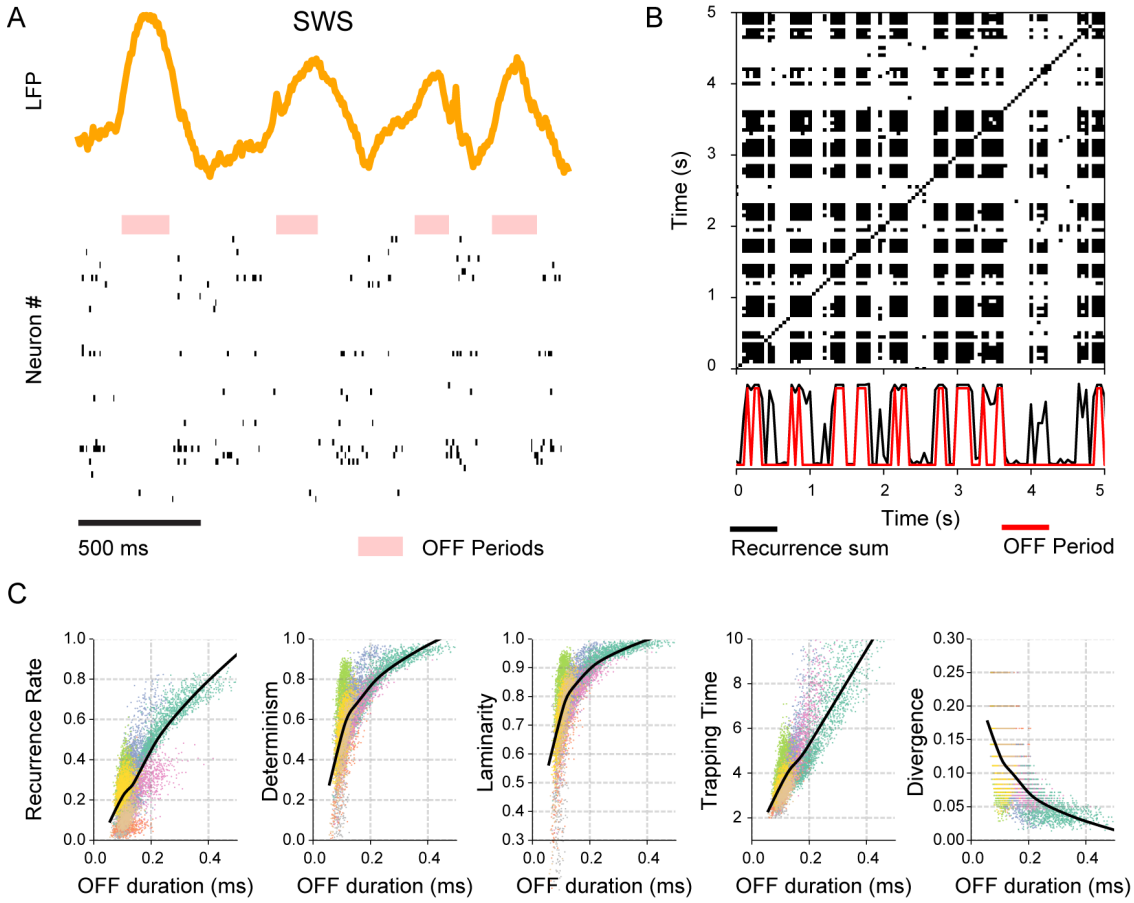

Figure 4: Correlation between recurrent spiking activity and OFF-periods in the neocortex during SWS. **A** Example of a local field potential and spiking activity for a representative animal, where OFF-periods are highlighted by shaded areas. **B** Corresponding recurrence plot, where the number of recurrences in time (sum over columns) is shown in the bottom panel together with the OFF-periods (shaded areas from panel **A**). **C** Correlation between RQA metrics – as those in Fig. 3 – and OFF-period's average duration; solid lines indicate the LOWESS regression estimate and colours indicate different sessions.

From the example in Fig. 4**B**, we can see that OFF-periods (red curve) match the times when recurrent trajectories are in a trapped state (black curve). In general, we find a significant correlation between the time-series of OFF-periods and that of the trapped recurrences: $R = 0.766 \pm 0.02$, with $P = 0$ (lower than the 64-bit computer's float-point) for all sessions. This means that $\sim$ 75% of the SWS trapped-recurrences

capture OFF-period dynamics, while the remaining $\sim$ 25% is comparable to the Wake/REM recurrences.

In particular, we find that all RQA metrics correlate with the mean duration of OFF-periods (Fig. 4**C**). The reason for this is that, the longer the system spends in an OFF-period, the more it stays trapped in a recurrent state, which translates to square-like patterns in the recurrent plots. This implies that RR, DET, LAM, and TT are positively correlated with the OFF-period average duration (Fig. 4**C**). On the other hand, because of the trapped recurrences, the unpredictability of the system decreases, resulting in a negatively correlated DIV with the OFF-period average duration (Fig. 4**C**). Overall, $P < 1 \times 10^{-2}$ for the linear regression of the different sessions. However, as can be seen from the locally-weighted scatter-plot smoothing (LOWESS) regression (continuous lines), some RQA metrics and the OFF-periods average-duration have a non-linear relationship, which is revealed by the departure from a straight line of DET, LAM, and DIV. In support of these results, we highlight that if we calculate RQA during SWS excluding OFF-periods (i.e employing the ON-periods), we find that the complexity reduction is lost (Fig.S3).

OFF-periods account for the loss of complexity in field recordings

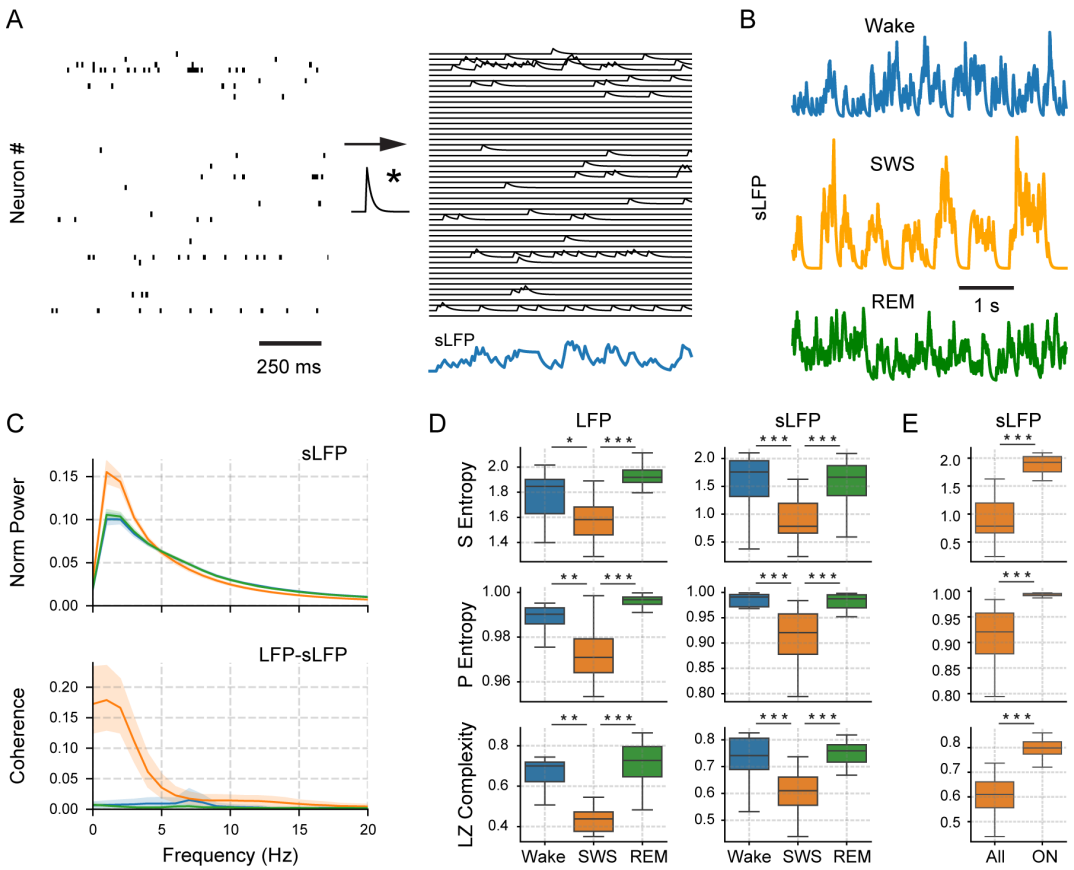

Figure 5: Synthetic local field potential (sLFP) creation and analysis during the states of Wake, SWS, and REM. A Example of the sLFP creation. A convolution between the binary raster plot of excitatory neurons and a decreasing exponential function is carried to obtain a continuous representation of the neuronal activity. The ensemble average is the sLFP (bottom signal). **B** Resultant sLFP examples for the states of Wake, SWS, and REM. **C** sLFP power spectra (top panel) and coherence between sLFP and LFP (bottom panel) for the different sleep-wake states. **D** Population values for Sample Entropy (top), Permutation Entropy (middle), and Lempel-Ziv Complexity (bottom) of the LFPs and sLFPs. **E** sLFP complexity metrics for SWS signals containing OFF and ON periods (All), and SWS containing only ON-periods (ON). $* = P < 0.05$, $** = P < 0.01$, $*** = P < 0.001$

To improve our understanding of previously reported results from field recordings, such as EEG, ECoG, or LFP [2, 3, 5, 8–12, 14], we create synthetic local field-potentials, sLFP, and compare them with LFP recordings (Fig. 5). We construct sLFP from the spiking activity of excitatory neurons (LFPs primarily reflect dendritic excitatory post-synaptic potentials [33]), assuming that each spike generates an exponentially decreasing post-synaptic potential (PSP) (Fig. 5**A**), and that the field activity arises from the average PSPs. Namely, we average the PSPs over the population of neurons at each time in order to obtain the instantaneous sLFP. This is known as the forward problem [22].

We find that sLFPs have asynchronous low-amplitude activity during Wake and REM sleep, but have synchronous activity during SWS, showing periodic high-amplitude waves occurring once or twice per second (Fig. 5**B**). Also, we find that the spectral content of the sLFP is similar to that of real LFPs, which can be seen in Fig. 5**C**. In particular, SWS has prominent delta oscillations (1-4 *Hz*), which are coherent to real LFP delta oscillations (Fig. 5**C** bottom). Thus, our sLFP construction recovers important LFP features across the sleep-wake states.

In order to validate the temporal-complexity of our sLFP, we quantify Sample Entropy (SE), Permutation Entropy (PE) and Lempel-Ziv Complexity (LZ) [1–5, 7–13, 26], and compare it with that from LFP recordings. In what follows, we will refer to them just as temporal complexity, since their resultant changes across states are nearly identical; statistics are reported in tables S3,S4.

Results from this quantification are shown in Fig. 5**D**. Firstly, we confirm that LFP activity is significantly less complex during SWS than during REM or Wake, which can be seen from the box-plots in the left panels of Fig 5**D**. These results are consistent with previously reported results for EEG and ECoG data [3, 10–12, 14]. Secondly, we obtain similar temporal complexity values for the sLFP, which can be seen in the right panels of Fig. 5**D**. We find that sLFPs also decrease significantly their complexity during SWS. Finally, we test whether OFF-periods are necessary for the complexity reduction during SWS. Hence, we construct sLFPs only employing SWS ON-periods; namely, excluding all OFF-periods. Panel **E** in Fig. 5 shows that when we analyse only the ON-period sLFP, the decrease in complexity during SWS is lost. In fact, ON-period SWS has significantly higher levels of complexity than SWS containing OFF-periods, which are comparable to those from Wake or REM states. Therefore, we conclude that OFF-periods are necessary for the complexity reduction observed in field recordings.

Universal avalanches govern the periods of activity across the sleep-wake states

Our results (Figs. 3, 4, and 5) show that the temporal complexity of the cortex decreases during SWS due to the presence of OFF-periods. Here, we complement these results by analysing spike avalanches occurring outside OFF-periods, namely, during ON-periods (which, in principle, could also contribute to decreasing the complexity of SWS). We note that by definition, spike avalanches only happen during ON-periods.

Avalanches are cascades of activity in quiescent systems [25, 35–38], which in our case, correspond to a surge in spikes within a brain region. This means that an avalanche excludes any OFF-period. Specifically, an avalanche is initiated (start) by a time-bin that contains at least one spike, happening after a time-bin without spikes and lasting (finish) until another time-bin without spikes is reached. For example, Fig. 6**A** shows an ensemble of spike-trains exhibiting an avalanche, where the time-bin is defined by the average inter-spike interval (ISI). Two parameters are commonly used to characterise an avalanche: size, i.e., total number of spikes, and duration, i.e., time from start to finish. The avalanche statistics for each sleep-wake state are derived from the probability distribution of these parameters [35, 36], which can be seen in Fig. 6**B**.

Our findings show minimal differences between the probability distribution of avalanches' duration or size during Wake, REM sleep, or SWS (left and middle panels of Fig. 6**B**). More importantly, these distributions collapse to the same scaling function (right panel of Fig. 6**B**). This implies that the spiking activity during ON-periods has a universal behaviour, independently of the sleep-wake state. In particular, the scaling function for the neuronal spiking avalanches approximates a power-law behaviour, which can be characterised by its exponent, $1/\sigma\nu z$. We find that $\frac{1}{\sigma\nu z} = 1.11$ for all sleep-wake states (inter-quartile range, $IQR = 0.05$) with $P = 0.21$, implying that differences between sleep-wake states are not significant. Similarly, the probability distributions of avalanche duration and avalanche size also follow power-laws with exponents τ and τ_t, respectively. These exponents are related by $\frac{\tau_t-1}{\tau-1}$, which for the cortex neurons and all sleep-wake states is $\frac{\tau_t-1}{\tau-1} = 1.19$ ($IQR = 0.33$, with $P = 0.31$).

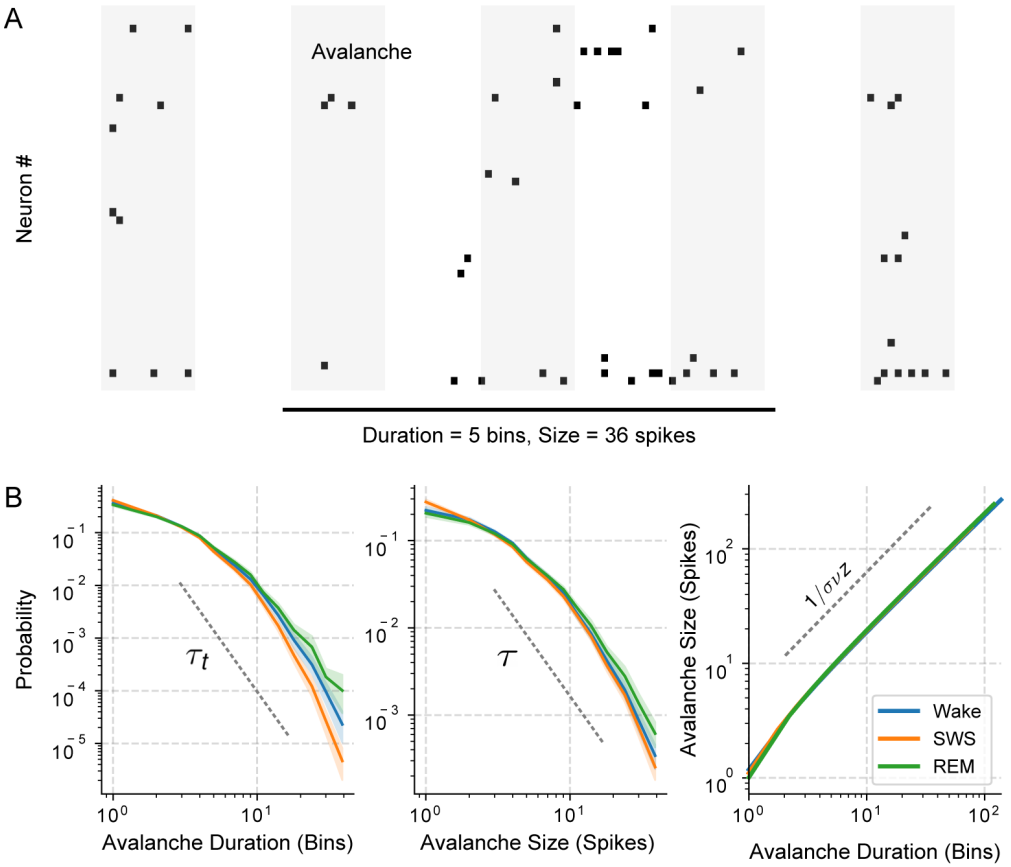

Figure 6: Avalanche statistics for the states of Wake, SWS and REM. A Example of how to compute a neural avalanche from a raster plot. The average inter-spike interval (ISI) is used to bin (shaded areas) the raster plot to count the number of spikes per bin. **B** Left: Distribution of avalanche duration for each state, where we estimate a τ_t exponent. Middle: Distribution of avalanche size for each state, where we estimate a τ exponent. Right: The size of each avalanche as a function of its duration for each state, where we estimate the $\frac{1}{\sigma\nu z}$ exponent. Distribution mean (solid lines) and 95% confidence interval (shaded areas).

We also calculate the branching parameter for the avalanches in each state. This parameter quantifies how spikes propagate during an avalanche, measuring the average of the number of spikes at time $t+1$ given a single spike at time t, i.e., $\sigma = \frac{1}{N}\sum(spikes(t+1) \mid spikes(t) = 1)$ [25]. The branching parameter (σ) yields a median of $\sigma = 1.01 \pm 0.01$, without differences across states ($P = 0.11$). Same as with the avalanche statistics during SWS, we calculate the branching parameter excluding OFF-periods (in order to avoid isolated OFF-period spikes) [31].

These results show that complexity differences in the sleep-wake states originate primarily from the distribution of quiescence periods, i.e., OFF-periods. Particularly, studying the ON-periods we show that once the spiking activity is initiated, it follows an avalanche behaviour with a universal scaling relationship and irrespective of the sleep-wake state. These conclusions restrict the possible mathematical models that can be used to describe cortical-dynamics, since the model must be able to reproduce OFF-periods (during SWS) and the universal avalanches appearing during ON-periods (for any state). In particular, some models from Statistical Physics allow phase transitions (such as the Ising Model for the ferromagnetic transition), which are known to show universal behaviours and scaling functions close to the critical point (i.e., close to the phase transition). Such models have been shown to have similar exponents to the ones we find here [36].

Critical branching model for the spiking activity in the cortex

Our analyses of the *in-vivo* population activity in the rat's cortex show: that neurons can synchronise quiescent states by allowing OFF-periods to shape cortical activity during SWS, and that neurons can maintain highly complex patterns during active periods by allowing the emergence of avalanches with universal properties. Here, we test whether the avalanche statistics and the emergence of synchronously quiescent-periods can be captured by a critical branching model with the addition of an external source that periodically silences noise. We show that we can tune this model to balance the presence of diverse temporal-patterns (complexity), allowing to increase information-processing capabilities, and the synchronisation of quiescent periods (OFF-periods), allowing to have an optimal segregation of information. Our results complement those from the critical-brain hypothesis [25, 35–42], which assumes that brain activity self-organises (non-equilibrium) to a a critical point, naturally balancing information processing and transmission.

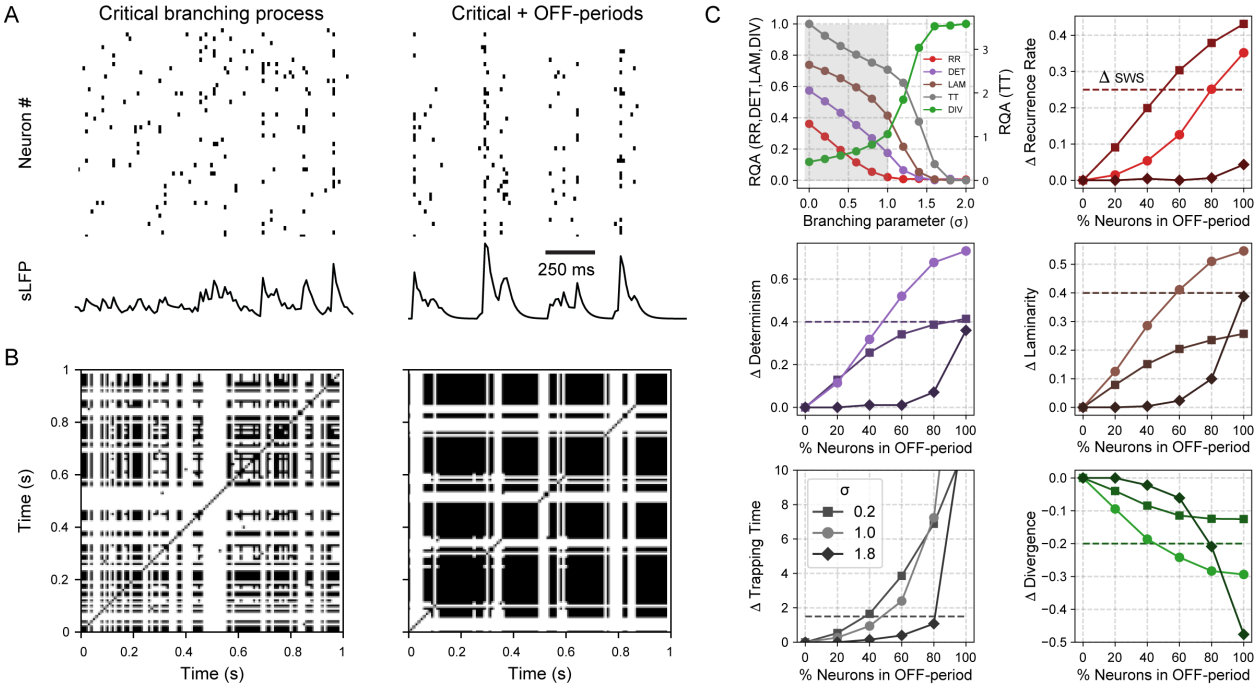

Figure 7: Modified critical branching model reproduces neuronal activity of Wake and SWS. A Population activity (raster plot) obtained from the model for 50 neurons and their synthetically generated local-field Potential (sLFP) (see Fig. 5). Left: model without noise silencing and tuned to its critical point, where the branching parameter $\sigma = 1$. Right: model tuned to $\sigma = 1$ with an external periodic-silencing of the noise. **B** Resultant recurrence plots for the data from panels **A**. **C** RQA metrics as function of σ and the percentage of neurons with the noise periodically silenced. Top left: RQA metrics for the (pristine) critical branching model as function of branching parameter σ (see Methods). Grey [white] band shows the sub-critical [super-critical] phase. Remaining panels: differences between RQA metrics for the model with and without periodic-silencing of the noise, Δ, as a function of the percentage of neurons having their noise silenced. Colours for Δ RQA metrics follow those from top left panel **C**. The horizontal dashed line shows the Wake-SWS difference for the experimental results. Note that in all cases, circles show the critical model

The critical branching model consists of interacting discrete units that evolve in time, whose internal state may be resting, spiking, or refractory; thus modelling the neuron's basic states. The branching parameter, σ, controls the probability of a spike from unit A at time t affects unit B at time $t + 1$. When $\sigma = 1$, the system is critical, having a phase transition from a sub-critical quiescent state for $\sigma < 1$ (activity dies out after a small transient) to a super-critical active state for $\sigma > 1$ (activity is self-sustained). The units evolve according to the excitation coming from neighbouring units as well as due to a noisy component (set by a Poisson distribution), which can randomly change the state of any unit at any given time. The interplay

between units interacting due to branching and the noisy substrate recreates a network of higher-order neurons that receives inputs from lower areas. Here, we add to the branching model a periodic silencing of the noise for some (adjustable percentage of) units in order to model delta waves and OFF-periods.

Figure 7**A** shows an example of the resultant spike trains for the branching model (left panel) and our modified version (right panel); that includes a periodic silencing of the Poisson noise. These results are obtained from using 50 units (similar size to the experimental ensembles recorded) and setting the branching parameter at the critical point: $\sigma = 1$, in agreement with the experimental value measured. Their respective recurrence plots are shown in Fig. 7**B**. On the modified branching model, we periodically silence the noise input arriving to a given set of units during a 250 *ms* interval (similar to Ref. [35]), and call it as Critical + OFF-periods. This external forcing is enough to drive the field activity to a synchronised state of quiescent inactivity (as can be seen from the sLFP on the right panel of Fig. 7**A**), trapping the population spiking-activity trajectories into recurrent square-like patterns (Fig. 7**B**), similar to the experimental results from the neocortex and hippocampus (see Fig. 2**B** and 3**A**). These qualitative results show that, when the critical branching model is set close to (or on) $\sigma = 1$, the model exhibits a similar spiking activity as Wake or REM sleep states. On the other hand, when a periodic silencing of the noise is added, then the critical branching model has similar traits to those from SWS state.

We use RQA metrics to quantify the differences between the branching model and the modified model having a periodic noise-silencing, where results are shown in Fig. 7**C**. The top left panel contains all RQA metrics for the branching model with 50 units as a function of σ, where the shaded area signals the sub-critical phase. These metrics would show a phase transition at $\sigma = 1$ when the number of units tends to infinity (i.e., at the thermodynamic limit), otherwise having smoother curves – as in this panel. For $\sigma = 1$, the model has RR$\simeq 0.02$, DET$\simeq 0.2$, LAM$\simeq 0.4$, DIV$\simeq 0.3$, and TT$\simeq 2.5$, which are comparable to the average RQA values of Figs. 2**C** and 3**B** corresponding to Wake and REM sleep states at different cortical locations containing $\simeq 45 \pm 5$ neurons. The remaining panels show the change in the RQA metrics when the periodic noise-silencing is added to the model – changes are shown as a function of the percentage of units having their noise periodically silenced. By a horizontal dashed line, we also include (as a reference) the SWS RQA metric relative to the critical branching model value. In other words, this relative SWS metric is found from taking the value obtained from the experimental average RQA metric shown in Fig. 3**B** and subtracting the critical branching model RQA metric from the top left panel in Fig. 7**C**. For example, during SWS, DET$\simeq 0.6$ for all cortical locations in Fig. 7**C**, while DET$\simeq 0.2$ for the critical branching model ($\sigma = 1$). Hence, the relative SWS value is ΔDET$\simeq 0.4$. Using this, we can find the percentage of units with periodically-silenced noise that are needed to recuperate the particular experimental values shown in Fig. 3**B**.

From the modified critical branching model, we find that as the number of units with an OFF-period increases, RQA metrics cross those observed during SWS from the *in-vivo* recordings (horizontal dashed-line). In particular, when the model dynamics is at the critical point, $\sigma = 1$, it is enough to apply a periodic noise-silencing to $40 - 60\%$ of the units to reproduce the RQA values during SWS (intersection of the Δ RQA metrics with the corresponding horizontal dashed-lines); with the exception of RR, which requires 80%. On the contrary, both the sub- and super-critical models need a considerably larger percentage to reproduce the observed SWS values – between $80 - 100\%$ (with the exception of RR). Therefore, these results imply that: i) the branching model needs to be close to $\sigma = 1$ to reproduce the recurrent properties observed during Wake or REM sleep from *in-vivo* extra-cellular recordings, and ii) that the inclusion of a periodic noise-silencing to $40 - 60\%$ of the units reproduces the recurrent properties observed during SWS.

Discussion

It has been widely reported the field recordings' complexity decreases during SWS [2, 3, 5, 8–12, 14]. From a neural activity, the reason behind this reduction remained elusive. Here, we show: i) that the presence of OFF-periods in neuronal population activity correlates with the complexity reduction of the LFP during SWS (Fig. 4); ii) that the existence of OFF-periods is necessary for this complexity reduction (Figs. 5 and 6); and iii) that introducing OFF-periods to a critical branching model is sufficient (enough) to reproduce the SWS characteristics from the *in-vivo* recordings (Fig. 7). In particular, we show (ii) by analysing synthetically generated LFPs without OFF-periods, which maintain complexity levels comparable to wakefulness or REM sleep, and by finding a universal behaviour for the spike avalanches' duration and size, which appears

during SWS ON-periods, REM sleep, and wakefulness. Overall, our findings suggest that when the cortex complex activity is is hindered by synchronous OFF-periods, consciousness fades.

Recurrence quantification analysis and persistent homology

Our work is focused on the analysis of spiking activity from *in-vivo* population recordings during the main sleep-wake states and at different cortical locations (Figs. 2 and 3). We employ RQA to retrieve the main dynamical features of the population activity from a $2D$ recurrence plot and quantify its complexity (Fig. 1). A significant advantage of RQA over methods that require dimensionality-reduction algorithms, is that RQA is robust to parameter tuning (e.g changing the recurrence tolerance or the spike count bin-width, Fig. S2), is computationally efficient (shorter time-series are sufficient, $10\,s$ windows are enough to find differences between states), and it keeps results and interpretations clear.

We note that RQA has parallelisms to topological data-analysis, such as persistent homology, which relies on studying the topology of the high-dimensional cloud of points (manifold) that the system's evolution creates in phase-space [43]. For example, persistent homology has been applied to neurons from the anterior nucleus of the thalamus, showing that a ring structure appears in phase space during Wake and REM sleep but is lost during SWS [43]. However, when we apply this method to our dataset (as can be seen from Fig. S4), we find no significant differences in the manifold's topology of the sleep-wake states ($P > 0.05$). The lack of similar findings suggests that the neocortex has a different phase-space attractor than that of the anterior nucleus, which is irreducible to a ring-like topology and instead looks like a cloud of points without any simple low-dimensional feature (see Fig. S4).

OFF-periods reduce the complexity of cortical activity during SWS

We find that the evolution of the population spiking activity within its manifold is significantly altered during SWS, in contrast to the unchanged attractor's topology. In particular, we show that the alteration of the cortex's dynamics during SWS is due to the presence of population OFF-periods, which are observed as synchronous silences between neurons (i.e., quiescent activity in Fig. 4). For example, one can think that the spiking activity at any location in the cortex during Wake, REM sleep, and SWS states can start at a similar location in phase space. However, as the population activity evolves and a trajectory is traced for each of the sleep-wake states, the SWS's trajectory is the only one attracted to the origin whenever an OFF-period appears (zero population activity) [29, 31, 45, 46]. Namely, OFF-periods disrupt the spiking activity during SWS, bypassing the causal interactions between neurons [26–28].

By showing that OFF-periods reduce the complexity of neocortical activity during SWS, we can explain two different observations. On the one hand, slow waves ($0.1 - 1\,Hz$) and delta waves ($1 - 4\,Hz$) have been associated to the loss of complex neuronal-interactions during sleep [26–28]. This observation is consistent with our power spectrum and coherence results (see Fig. 5**C**), which further confirms the relationship between OFF-periods and delta waves [29, 34, 45]. Moreover, it was speculated that the nature of the undergoing oscillation (theta vs slow waves) could constrain the firing pattern repertoire and its complexity [44]. We confirm this idea, showing that the oscillation's neural substrate determines complexity. On the other hand, it has been shown for individual neurons that the complexity of firing patterns decreases during SWS [5]. This decrease can be explained by the OFF-periods, as their appearance causes neurons to remain silent during synchronous intervals of quiescent activity, making their overall firing-patterns less complex. However, we note that when analysing the firing patterns of our neurons independently (Supplementary Material), we find that a considerable number of neurons maintain a complex pattern even during SWS (see Fig. S7). Therefore, we argue that the complexity reduction is in fact a population-level phenomena. In support of this idea, we show that the complexity differences between Wake or REM sleep and SWS increase as the number of simultaneously recorded neurons grows (see Fig. S5).

It is important to note that we also observe a reduction in complexity during SWS for the neurons from the hippocampus, in spite of being an area without OFF-periods [47]. The population activity of the hippocampus during SWS oscillates between periods of decreased spiking activity (almost quiescent) and bursts of spiking activity (during sharp-wave ripples). This alternation in the firing patterns has been called bi-stability, or excitability, and is also a common trait to neocortical sleep [47]. Therefore, in both areas, the change in their respective population-dynamics correlates to the complexity reduction during SWS.

Measuring complexity from field recordings

The complex nature of brain activity, and its reduction during unconscious's states, has been extensively reported using classical neuroscience approaches [48,49]. In particular, the power spectrum of field recordings has been shown to exhibit a power-law decay, $f^{-\alpha}$, for a broad frequency range f, similar to a $f^{-1} = 1/f$ pink noise. Recently, it has been shown that the exponent governing such decay becomes smaller than 1 (i.e., a more pronounced decay) during sleep and anaesthesia [48, 49]. We confirm this finding on power-spectra from field recordings of LFPs and electrocorticograms, ECoGs (see Fig. S6). We find similar decay exponents during SWS and REM sleep ($\alpha_{sleep} \simeq 2$), which differ from wakefulness's power-spectrum decay. Also, we note that the difference in the exponents is significantly higher in ECoGs, where $\alpha_{wake} \simeq 1$, than in LFPs, where $\alpha_{wake} \simeq 2$ as during sleep. This could be suggesting the presence of extra-neural sources during wakefulness that alter the ECoG recordings power-spectrum decay, but disappear at the LFP recording level. However, further research is required.

These observations are also consistent with our RQA of the rat's cortex neuronal activity. We justify that OFF-periods are responsible for reducing the complexity of field recordings during SWS by generating synthetic field recordings from the population activity (Fig. 5). From this synthetically constructed LFP, we see that complexity reductions during SWS are lost when we eliminate the OFF-periods from the construction (see Fig. 5**E**). Because OFF-periods and delta waves promote the appearance of low frequencies, it is expected that the power-spectrum decay becomes steeper (i.e., α grows).

Spiking periods show universal dynamics across states

An important result that we find is that the population dynamics during SWS's ON-periods is indistinguishable to the population dynamics during Wake or REM sleep. This strengthens our claim, that OFF-periods are mainly responsible for the change in SWS complexity. As our results from RQA (Fig. 4,S3), field complexity metrics (Fig. 5), and avalanche statistics (Fig. 6) show, while spiking activity is occurring (i.e., during ON-periods), SWS behaves exactly as (if not more complex than) Wake or REM sleep.

Specifically, we show that neuronal avalanches of length t contain an average of $f(t)$ spikes, where f is an scaling function independent of the sleep-wake state.This means that these avalanches from the frontal cortex of rats, follow a universal behaviour, which was previously reported in the visual cortex [35]. We find that the scaling exponent ($\frac{1}{\sigma\nu z} = 1.11$) and the exponent relating the avalanche statistics ($\frac{\tau_t - 1}{\tau - 1} = 1.19$) are relatively similar, which is an expected relationship when a system is close to criticality [36]. Therefore our results support the hypothesis that complex cortical activity arises from near-critical dynamics [36, 40].

OFF-periods are sufficient to reproduce the complexity reduction in a critical model of the cortex

To complement our results justifying that OFF-periods reduce the complexity of cortical activity, we show that their introduction into a cortical model is sufficient to generate a decrease in complexity. Hence, we first show that a critical branching model recovers the experimental RQA values during Wake/REM. Then, we periodically silence the noise that is inherent to the model as we observe the RQA change, mimicking SWS activity. This periodic silence reproduces OFF-periods, which are generated from pre-synaptic inhibition into principal cells of the cortex [50].

We find that near the critical point of the model, the percentage of neurons we need to force to get a SWS-like state is optimal with respect to either the sub- or super-critical state. For instance, silencing the input to $40 - 60\%$, creates a complexity reduction similar to that observed experimentally. This further adds to the idea of criticallity in the brain, which would explain the increased complexity [24], information processing and transmission [25], and dynamical range [39].

Methods

Datasets

We analyse three datasets: Watson et al. (Population activity neocortex, available at http://crcns.org/data-sets/fcx/fcx-1) [51], Grosmark and Buzsaki (Population activity hippocampus, available at http://crcns.org/data-sets/hc/hc-11) [52], and Gonzalez et al 2019 [10] (ECoG neocortex, available at request). The reader is referred to the original publications for full details of the experimental methods. We provide a summary below.

For the frontal cortex dataset, silicon probes were implanted in frontal cortical areas of 11 male Long Evans rats. Recording sites included medial prefrontal cortex (mPFC), anterior cingulate cortex (ACC), premotor cortex/M2, and orbitofrontal cortex (OFC). Recordings took place during light hours in the home cage (25 sessions, mean duration of 4.8 hs $\pm$ 2.2 std). We note that we exclude *BWRat19_032413* from the analysis, as it did not contain REM sleep. Data was sampled at 20 kHz. To extract LFPs, recordings were lowpassed and resampled at 1250 Hz. To extract spikes, data was highpass filtered at 800 Hz, and then threshold crossings were detected. Spike sorting was accomplished by means of the KlustaKwik software. Sleep-wake states were identified by means of principal component analysis. SWS exhibited high LFP PC1 (power in the low $<$20 Hz) and low EMG. REM sleep showed high theta/low EMG cluster, and a diffuse cluster of low broadband LFP with higher EMG. Wake showed a diffuse cluster of low broadband LFP, with higher EMG, and a range of theta. OFF periods were extracted as periods of population silence lasting at least 50 ms and no more than 1250 ms. Conversely, ON periods consisted of periods of population firing between OFF periods with at least 10 total spikes and lasting 200-4000ms. For a further description of these methods, see [51].

For the hippocampal dataset, silicon probes were implanted in the dorsal hippocampus (CA1) of 4 male Long Evans rats (7 recordings total). LFP and spikes were extracted similarly to the cortical dataset. A similar criterion as before was employed to identify the sleep-wake states; for a full description, see [53].

For the ECoG dataset, 12 animals with 7 steel screw electrodes placed intracranially above the dura matter were analysed. The recorded areas included motor, somatosensory, visual cortices (bilateral), the right olfactory bulb, and cerebellum, which was the reference electrode. Data was sampled at 1024 Hz, employing a 16 bits AD converted. The states of sleep and wakefulness were determined in 10-s epochs. Wake was defined as low voltage fast waves in the motor cortex, a strong theta rhythm (4-7 Hz) in the visual cortices, and relatively high EMG activity. NREM sleep was determined by the presence of high voltage slow cortical waves together with sleep spindles in motor, somatosensory, and visual cortices associated with a reduced EMG amplitude; and REM sleep as low voltage fast frontal waves, a regular theta rhythm in the visual cortex, and a silent EMG except for occasional twitches. Additional visual scoring was performed to discard artefacts and transitional states.

Recurrence quantification analysis

Prior to analysing the recurrences [32, 54, 55], we bin the spike data to 50-ms firing count bins.

Given a system $X = [\vec{x}(t1), \vec{x}(t2), ..., \vec{x}(tn)]$ formed by the distinct time measurements of the vector $\vec{x}$, whose entries are the different elements of the system, a recurrence plot is formed creating a matrix R whose entries are given by:

$$\begin{cases} R(i,j) = 1 & \left\| \vec{x}(i) - \vec{x}(j) \right\| \leq \epsilon \\ R(i,j) = 0 \end{cases} \tag{1}$$

.

Where $\epsilon > 0$ is the accepted tolerance level. Thus, a recurrence between two time points would only occur if the system was located in a similar region (state) of the phase space at the respective times (up to an error of ϵ). In our case, ϵ was set to 1 standard deviation of the population firing rate (spikes were summed across neurons)

To quantify the patterns arising from recurrence plots, we employed common measures form recurrence quantification analysis (RQA). The metrics employed (defined below) were: recurrence rate (RR),

determinism (DET), laminarity (LAM), trapping time (TT) and divergence (DIV)

$$RR = \frac{1}{N^2}\sum_{i,j=1}^{N} R_{i,j} \tag{2}$$

$$DET = \frac{\sum_{l=l_{\min}}^{N} lP(l)}{\sum_{l=1}^{N} lP(l)} \tag{3}$$

$$LAM = \frac{\sum_{v=v_{\min}}^{N} vP(v)}{\sum_{v=1}^{N} vP(v)} \tag{4}$$

$$TT = \frac{\sum_{v=v_{\min}}^{N} vP(v)}{\sum_{v=v_{\min}}^{N} P(v)} \tag{5}$$

$$DIV = \frac{1}{Lmax} \tag{6}$$

Where $P(l)[P(v)]$ indicate the probability of finding a diagonal [vertical] line of length $l[v]$, and $Lmax$ indicates the longest diagonal line, excluding the identity line.

Synthetic LFPs and field complexity measures

To construct the sLFP, we convolve the spike times (binned into a 125 Hz sampling frequency) of each excitatory neuron S_n by an exponentially decreasing kernel. Therefore, the convolved spikes C_n of the nth neuron are obtained as:

$$C_n(t) = S_n(t) * e^{\frac{-t}{\tau}} \tag{7}$$

where the symbol $*$ is the convolution operator and τ is the exponential time constant. The τ constant is set to 24 ms for all putative excitatory neurons, which is a reasonable mEPSP time-constant for a pyramidal neuron in the frontal cortex [57]. Note that this selection of τ is also validated internally, as it allows to recover important LFP features in the sLFP.

After carrying out the convolution for each neuron, the average is taken across the neurons to produce the sLFP.

$$sLFP(t) = \frac{1}{N}\sum_{n=1}^{N} C_n(t) \tag{8}$$

Where N is the total number of simultaneously recorded neurons.

We analyse the sLFPs frequency content by calculating its power spectral density by means of Welch's algorithm employing the *signal.welch* scipy python 3 function (https://www.scipy.org), setting a 1 sec moving Hanning window, no overlap, and a 1 Hz frequency resolution. To get the sLFP-LFP coherence, we employ the *signal.coherence* scipy function with the same parameters as the frequency spectrum. We note that the LFP is averaged across channels and downsampled to 125 Hz prior to estimating the coherence to the sLFP.

To quantify the sLFP and LFP time-series complexity, we employ thre metrics widely employed in the literature, namely Permutation Entropy, Sample Entropy and Lempel-Ziv Complexity [1–4, 7–12, 14]. We employ the *antroPy* python 3 package (https://github.com/raphaelvallat/antropy).

Permutation Entropy [56] consists in encoding a time-series $\{x(t),\ t = 1, \ldots, T\}$, by dividing it into $\lfloor (T - D)/D \rfloor$ non-overlapping vectors, where $\lfloor y \rfloor$ denotes the largest integer less than or equal to y and D is the vector length, which is much shorter than the time-series length ($D \ll T$). Then, each vector is classified according to the relative magnitude of its D elements, yielding an ordinal pattern (OP). For example, for $D = 2$, the vectors have only two possible OPs for any time t_i: either $x(t_i) < x(t_{i+1})$ or $x(t_i) > x(t_{i+1})$, which yield either the 0 or 1 symbol, respectively. In the present report we employ $D = 3$, and $\tau = 5$ (τ being the distance between succesive time-stamps in each vector, in our case each vector is then constructed as

$[x(t), x(t+5), x(t+10)]$). After this, the Shannon entropy (SE) [58] is computed to obtain the Permutation Entropy.

$$H(S) = -\sum_{\alpha \in S} p(\alpha) \log [p(\alpha)] \tag{9}$$

where $p(\alpha)$ is the probability of finding symbol α in the signal (among the set of symbols S) and the summation is carried over all possible symbols.

Similar to Permutation Entropy, Sample entropy consists of dividing a time-series $\{x(t),\ t = 1, \ldots, T\}$ into a series of D sized vectors ($X(i)$), noting that $D \ll T$. A distance function (d) is then applied to vector pairs (with different indexes, like $X(i), X(j)$), which in our case was the Chebyshev distance. From this A is obtained as $d[X_{m+1}(i), X_{m+1}(j)] < r$ and B as $d[X_m(i), X_m(j)] < r$. Sample entropy is then defined as: $SampEn = -log(\frac{A}{B})$ In our case $D = 3$, note that we downsample the signals by a factor of 5, in order to match the permutation entropy τ.

Lastly, we employ the Lempel-Ziv complexity algorithm. Prior to apply this function, we binarized the sLFP signals by its mean value. Meaning that all time-points above the signal's mean are converted to a 1 and all below to a 0. After that the Lempel-Ziv complexity is estimated counting the the number of different substrings encountered as the sequence is viewed from beginning to the end. Then we normalise it as $LZn = \frac{\#substrings}{n/log(n)}$, making the metric less dependent on the signal's length.

Single neuron complexity measures

To quantify the complexity of the firing patterns of single neurons, we employ two different strategies, the Lempel-Ziv complexity of the raster plots and the inter-spike intervals (ISIs) entropy. For the ISI entropy, we construct the ISI histogram employing 18 bins equally spaced between 0 and 800 ms. After that, the Shannon entropy is computed as mentioned above. We note that we compute the Lempel-Ziv complexity as defined in the previous section.

Neuronal avalanches

To study scaling relationships in population dynamics, we quantify neuronal avalanches following previous studies [35, 36]. First multy-unit activity is binned, employing the average ISI. Then, we measure the time and number of spikes between one empty bin (lacking spikes) to the following empty bin. The duration of the avalanche is the number of bins it spans, and its size the number of spikes it contains. From these two quantities, the probability distributions are derived. We use the *powerlaw* (https://pypi.org/project/powerlaw/1.3.4/) python 3 package to construct these distributions and obtain their exponents (τ_t and τ). We compute the average number of spikes as a function of the avalanche duration to obtain the scaling relationships across states. From this function we obtain the exponent $\frac{1}{\nu\sigma z}$ by means of an ordinary least square fit on a log-log scale. We also calculate the branching parameter for the avalanches in each state, measuring the average of the number of spikes at time $t+1$ given a single spike at time t, i.e., $\sigma = \frac{1}{N} \sum (spikes(t+1) \mid spikes(t) = 1)$ [25].

Critical branching model

The critical branching model consists of 50 interacting units randomly connected in a Erdos-Renyi topology (each pair of neurons has a 0.01 probability to be connected). Each unit has 3 possible states: resting, firing or refractory. The transition between resting and firing can either occur from the excitation coming from a connected neuron firing in the preceding time, or by the intrinsic Poisson noise that each neuron receives independently. The Poisson noise is set by generating a random matrix whose values come from a $[0, 1]$ uniform distribution, and then setting for each entry a spike if the value is less than $1 - e^{-\lambda}$ ($\lambda = 0.014$). Once a neuron fires, it goes deterministically to the refractory state, in which it cannot be excited either from a connected neuron or from the Poisson noise. After 1 step in a refractory state, each neuron goes to the resting state and becomes excitable again. The interaction among neurons is controlled by the branching parameter (σ), which regulates the overall excitability of the system. For instance, if neuron i fires, the probability that a neighbouring unit fires is defined as $P_{prop} = \sigma / \overline{D_i}$, where $\overline{D_i}$ is the average node degree for

unit i. To obtain the plots shown in Fig. 7, we employ 1 million iterations from each network, and average the results over 100 trials. To obtain a SWS state, we periodically silenced the Poisson noise coming to the network in a 250*ms* step with a 4*Hz* frequency.

Persistent homology

To study the topology of the neural manifolds during the states of sleep and wakefulness, we employ similar procedures as [43]. Briefly, we bin the spike data to 100-ms firing count bins and then reduce its dimensionality by means of the isomap algorithm to a 3d representation. After that, we calculate persistent homology by means of the *ripser* python3 package, limiting the analysis to Betti 0 and 1 numbers. To compare between conditions, we select the most persistent Betti 0 and 1 components for each session in each state.

Statistics

We present data as regular boxplots showing the median, the 1st and 3rd quartiles, and the distribution range. Because of the complexity metrics we analyse, we employ non-parametric statistics. In particular we use the Friedman test (available with the *scipy.stats*) to compare the results among states (Wake-SWS-REM) with the Siegel post-hoc test applying the Benjamini-Hochberg false discovery rates correction (available with the *scikitlearn* python 3 package (https://scikit-learn.org/stable/)) . We set $P < 0.05$ for a result to be considered significant. In addition to P-values, we also reprt Cohen's d, which quantifies the magnitude of a result in terms of a standardised difference between conditions, considering an effect size to be large if Cohen's d is > 0.8.

For the power spectrums and avalanche results we present the data as the mean with the 95% confidence interval (obtained through bootstrap sampling). For the correlation analysis, we employ LOWESS regression to fit the best estimate to the scatter plot, by means of the regplot function available at *seaborn* (https://seaborn.pydata.org) python 3 function. As LOWESS regression doesn't have an associated *P* value, we employ a linear regression for each session and report the result significant only if $P < 0.05$ for all sessions. Additionally, to correlate the OFF-periods to the recurrence sum, we employ the point-biserial correlation *pointbiserialr* available at *scipy* https://scipy.org.

Code availability

The codes developed to analyse population activity recurrences are freely available at `https://github.com/joaqgonzar/Recurrence_population_activity`, including the recurrence functions and jupyter notebook examples.

Acknowledgements

JG acknowledges the support of Comisión Académica de Posgrado (CAP), CSIC Iniciación and PEDECIBA. PT also acknowledges the support of PEDECIBA. ABLT acknowledges the support of CAPES and CNPq.

References

[1] Jordan,D., Stockmanns,G., Kochs,E,B., Pilge, S., & Schneider, G. Electroencephalographic Order Pattern Analysis for the Separation of Consciousness and Unconsciousness: An Analysis of Approximate Entropy, Permutation Entropy, Recurrence Rate, and Phase Coupling of Order Recurrence Plots. *Anesthesiology*.**109(6)**:1014-1022. 2008.

[2] Ouyang, G., Dang, C., Richards, D. A., & Li, X. Ordinal pattern based similarity analysis for EEG recordings. *Clinical Neurophysiology* **121(5)**: 694-703 (2010).

[3] Nicolaou, N., & Georgiou, J., The use of permutation entropy to characterize sleep electroencephalograms *Clinical EEG and Neuroscience* **42** 24-28 (2011).

[4] Sitt, J,D., King J,R., Karoui, I,E., Rohaut, B., Faugeras, F., Gramfort, A., Cohen, L., Sigman, M., Dehaene, S., & Naccache, L. Large scale screening of neural signatures of consciousness in patients in a vegetative or minimally conscious state. *Brain*.**137(8)**:2258–2270. 2014.

[5] Abasolo D, Simons S, Morgado da Silva R, Tononi G, Vyazovskiy VV. Lempel-Ziv complexity of cortical activity during sleep and waking in rats. J Neurophysiol. 2015 Apr 1;113(7):2742-52. doi: 10.1152/jn.00575.2014. Epub 2015 Feb 25. PMID: 25717159; PMCID: PMC4416627.

[6] Sarasso S, Boly M, Napolitani M, Gosseries O, Charland-Verville V, Casarotto S, Rosanova M, Casali AG, Brichant JF, Boveroux P, Rex S, Tononi G, Laureys S, Massimini M. Consciousness and Complexity during Unresponsiveness Induced by Propofol, Xenon, and Ketamine. Curr Biol. 2015 Dec 7;25(23):3099-105. doi: 10.1016/j.cub.2015.10.014. Epub 2015 Nov 19. PMID: 26752078.

[7] Thul, A., Lechinger, J., Donis, J., Michitsch, G., Pichler, G., Kochs, E,F., Jordan, D., Ilg, R., & Schabus M. EEG entropy measures indicate decrease of cortical information processing in Disorders of Consciousness. *Clin Neurophysiol*. **127(2)**:1419-1427. 2016.

[8] Schartner MM, Pigorini A, Gibbs SA, Arnulfo G, Sarasso S, Barnett L, Nobili L, Massimini M, Seth AK, Barrett AB. Global and local complexity of intracranial EEG decreases during NREM sleep. Neurosci Conscious. 2017 Jan 25;2017(1):niw022. doi: 10.1093/nc/niw022. PMID: 30042832; PMCID: PMC6007155.

[9] Bandt, C., A New Kind of Permutation Entropy Used to Classify Sleep Stages from Invisible EEG Microstructure. *Entropy* **19**(197), 1-12 (2017).

[10] González J, Cavelli M, Mondino A, Pascovich C, Castro-Zaballa S, Torterolo P, Rubido N. Decreased electrocortical temporal complexity distinguishes sleep from wakefulness. Sci Rep. 2019 Dec 5;9(1):18457. doi: 10.1038/s41598-019-54788-6. PMID: 31804569; PMCID: PMC6895088.

[11] González J, Cavelli M, Mondino A, Pascovich C, Castro-Zaballa S, Rubido N, Torterolo P (2020). Electrocortical temporal complexity during wakefulness and sleep: an updated account. Sleep Science (Special Edition), DOI: 10.5935/1984-0063.20200013

[12] Hou F, Zhang L, Qin B, Gaggioni G, Liu X, Vandewalle G. Changes in EEG Permutation Entropy in the evening and in the transition from wake to sleep. Sleep. 2020 Nov 7:zsaa226. doi: 10.1093/sleep/zsaa226. Epub ahead of print. PMID: 33159205.

[13] Varley TF, Sporns O, Puce A, Beggs J. Differential effects of propofol and ketamine on critical brain dynamics. PLoS Comput Biol. 2020 Dec 21;16(12):e1008418. doi: 10.1371/journal.pcbi.1008418. PMID: 33347455; PMCID: PMC7785236.

[14] Mondino A, Hambrecht-Wiedbusch VS, Li D, York AK, Pal D, González J, Torterolo P, Mashour GA, Vanini G. Glutamatergic Neurons in the Preoptic Hypothalamus Promote Wakefulness, Destabilize NREM Sleep, Suppress REM Sleep, and Regulate Cortical Dynamics. J Neurosci. 2021 Apr 14;41(15):3462-3478. doi: 10.1523/JNEUROSCI.2718-20.2021. Epub 2021 Mar 4. PMID: 33664133.

[15] Tononi G, Edelman GM. Consciousness and complexity. Science. 1998 Dec 4;282(5395):1846-51. doi: 10.1126/science.282.5395.1846. PMID: 9836628.

[16] Oizumi., M, Albantakis., L, & Tononi, G. From the Phenomenology to the Mechanisms of Consciousness: Integrated Information Theory 3.0 *PLoS Comput Biol* **10(5)**:e1003588. 2014.

[17] Agerholm ED, Scott G, Shew WL, Song C, Leech R, Knöpfel T, Sharp DJ. Cortical Entropy, Mutual Information and Scale-Free Dynamics in Waking Mice. Cereb Cortex. 2016 Oct;26(10):3945-52. doi: 10.1093/cercor/bhw200. Epub 2016 Jul 6. PMID: 27384059; PMCID: PMC5028006.

[18] Croce, P., Quercia, A., Costa, S & Zappasodi Circadian Rhythms in Fractal Features of EEG Signals. *Frontiers in Physiology* **9**:1567. (2018)

[19] Shumbayawonda E, Tosun PD, Fernández A, Hughes MP, Abásolo D. Complexity Changes in Brain Activity in Healthy Ageing: A Permutation Lempel-Ziv Complexity Study of Magnetoencephalograms. Entropy (Basel). 2018;20(7):506. Published 2018 Jul 3. doi:10.3390/e20070506

[20] Gomez C, Hornero R, Abasolo D, Lopez M, Fernandez A. Decreased Lempel-Ziv complexity in Alzheimer's disease patients' magnetoencephalograms. Conf Proc IEEE Eng Med Biol Soc. 2005;2005:4514-7. doi: 10.1109/IEMBS.2005.1615472. PMID: 17281242.

[21] Pal D, Li D, Dean JG, et al. Level of Consciousness Is Dissociable from Electroencephalographic Measures of Cortical Connectivity, Slow Oscillations, and Complexity. J Neurosci. 2020;40(3):605-618. doi:10.1523/JNEUROSCI.1910-19.2019

[22] Nunez P, Srinivasan, R. Electric fields of the brain: The neurophysics of EEG. Second edition. Oxford University Press. 2006.

[23] Whitham, E. M., Pope, K. J., Fitzgibbon, S. P., Lewis, T., Clark, C. R., Loveless, S., Broberg, M., Wallace, A., DeLosAngeles, D., Lillie, P., Hardy, A., Fronsko, R., Pulbrook, A. & Willoughby, J. O. Scalp electrical recording during paralysis: Quantitative evidence that EEG frequencies above 20 Hz are contaminated by EMG. *Clin Neurophysiol* **118** 1877-1888 (2007)

[24] Timme NM, Marshall NJ, Bennett N, Ripp M, Lautzenhiser E, Beggs JM. Criticality Maximizes Complexity in Neural Tissue. Front Physiol. 2016 Sep 27;7:425. doi: 10.3389/fphys.2016.00425. PMID: 27729870; PMCID: PMC5037237.

[25] Beggs JM, Plenz D. Neuronal avalanches in neocortical circuits. J Neurosci. 2003 Dec 3;23(35):11167-77. doi: 10.1523/JNEUROSCI.23-35-11167.2003. PMID: 14657176; PMCID: PMC6741045.

[26] Rosanova M, Fecchio M, Casarotto S, Sarasso S, Casali AG, Pigorini A, Comanducci A, Seregni F, Devalle G, Citerio G, Bodart O, Boly M, Gosseries O, Laureys S, Massimini M. Sleep-like cortical OFF-periods disrupt causality and complexity in the brain of unresponsive wakefulness syndrome patients. Nat Commun. 2018 Oct 24;9(1):4427. doi: 10.1038/s41467-018-06871-1. PMID: 30356042; PMCID: PMC6200777.

[27] D'Andola M, Rebollo B, Casali AG, Weinert JF, Pigorini A, Villa R, Massimini M, Sanchez-Vives MV. Bistability, Causality, and Complexity in Cortical Networks: An In Vitro Perturbational Study. Cereb Cortex. 2018 Jul 1;28(7):2233-2242. doi: 10.1093/cercor/bhx122. PMID: 28525544.

[28] Pigorini A, Sarasso S, Proserpio P, Szymanski C, Arnulfo G, Casarotto S, Fecchio M, Rosanova M, Mariotti M, Lo Russo G, Palva JM, Nobili L, Massimini M. Bistability breaks-off deterministic responses to intracortical stimulation during non-REM sleep. Neuroimage. 2015 May 15;112:105-113. doi: 10.1016/j.neuroimage.2015.02.056. Epub 2015 Mar 4. PMID: 25747918.

[29] Vyazovskiy VV, Olcese U, Lazimy YM, Faraguna U, Esser SK, Williams JC, Cirelli C, Tononi G. Cortical firing and sleep homeostasis. Neuron. 2009 Sep 24;63(6):865-78. doi: 10.1016/j.neuron.2009.08.024. PMID: 19778514; PMCID: PMC2819325.

[30] Nir Y, Staba RJ, Andrillon T, Vyazovskiy VV, Cirelli C, Fried I, Tononi G. Regional slow waves and spindles in human sleep. Neuron. 2011 Apr 14;70(1):153-69. doi: 10.1016/j.neuron.2011.02.043. PMID: 21482364; PMCID: PMC3108825.

[31] Todorova R, Zugaro M. Isolated cortical computations during delta waves support memory consolidation. Science. 2019 Oct 18;366(6463):377-381. doi: 10.1126/science.aay0616. PMID: 31624215.

[32] Norbert Marwan, M. Carmen Romano, Marco Thiel, Jürgen Kurths, Recurrence plots for the analysis of complex systems, Physics Reports, Volume 438, Issues 5–6, 2007, Pages 237-329, ISSN 0370-1573, https://doi.org/10.1016/j.physrep.2006.11.001.

[33] Buzsáki G, Anastassiou CA, Koch C. The origin of extracellular fields and currents–EEG, ECoG, LFP and spikes. Nat Rev Neurosci. 2012 May 18;13(6):407-20. doi: 10.1038/nrn3241. PMID: 22595786; PMCID: PMC4907333.

[34] Massimini M, Huber R, Ferrarelli F, Hill S, Tononi G. The sleep slow oscillation as a traveling wave. J Neurosci. 2004 Aug 4;24(31):6862-70. doi: 10.1523/JNEUROSCI.1318-04.2004. PMID: 15295020; PMCID: PMC6729597.

[35] Ribeiro TL, Copelli M, Caixeta F, Belchior H, Chialvo DR, Nicolelis MA, Ribeiro S. Spike avalanches exhibit universal dynamics across the sleep-wake cycle. PLoS One. 2010 Nov 30;5(11):e14129. doi: 10.1371/journal.pone.0014129. PMID: 21152422; PMCID: PMC2994706.

[36] Fontenele AJ, de Vasconcelos NAP, Feliciano T, Aguiar LAA, Soares-Cunha C, Coimbra B, Dalla Porta L, Ribeiro S, Rodrigues AJ, Sousa N, Carelli PV, Copelli M. Criticality between Cortical States. Phys Rev Lett. 2019 May 24;122(20):208101. doi: 10.1103/PhysRevLett.122.208101. PMID: 31172737.

[37] Bellay T, Klaus A, Seshadri S, Plenz D. Irregular spiking of pyramidal neurons organizes as scale-invariant neuronal avalanches in the awake state. Elife. 2015 Jul 7;4:e07224. doi: 10.7554/eLife.07224. PMID: 26151674; PMCID: PMC4492006.

[38] Ponce-Alvarez A, Jouary A, Privat M, Deco G, Sumbre G. Whole-Brain Neuronal Activity Displays Crackling Noise Dynamics. Neuron. 2018 Dec 19;100(6):1446-1459.e6. doi: 10.1016/j.neuron.2018.10.045. Epub 2018 Nov 16. PMID: 30449656; PMCID: PMC6307982.

[39] Kinouchi, O., Copelli, M. Optimal dynamical range of excitable networks at criticality. Nature Phys 2, 348–351 (2006). https://doi.org/10.1038/nphys289

[40] Chialvo, D. Emergent complex neural dynamics. Nature Phys 6, 744–750 (2010). https://doi.org/10.1038/nphys1803

[41] Meisel C, Olbrich E, Shriki O, Achermann P. Fading signatures of critical brain dynamics during sustained wakefulness in humans. J Neurosci. 2013 Oct 30;33(44):17363-72. doi: 10.1523/JNEUROSCI.1516-13.2013. PMID: 24174669; PMCID: PMC3858643.

[42] Scott G, Fagerholm ED, Mutoh H, Leech R, Sharp DJ, Shew WL, Knöpfel T. Voltage imaging of waking mouse cortex reveals emergence of critical neuronal dynamics. J Neurosci. 2014 Dec 10;34(50):16611-20. doi: 10.1523/JNEUROSCI.3474-14.2014. PMID: 25505314; PMCID: PMC4261090.

[43] Chaudhuri R, Gerçek B, Pandey B, Peyrache A, Fiete I. The intrinsic attractor manifold and population dynamics of a canonical cognitive circuit across waking and sleep. Nat Neurosci. 2019 Sep;22(9):1512-1520. doi: 10.1038/s41593-019-0460-x. Epub 2019 Aug 12. PMID: 31406365.

[44] Clawson W, Vicente AF, Ferraris M, Bernard C, Battaglia D, Quilichini PP. Computing hubs in the hippocampus and cortex. Sci Adv. 2019 Jun 26;5(6):eaax4843. doi: 10.1126/sciadv.aax4843. PMID: 31249875; PMCID: PMC6594769.

[45] Vyazovskiy VV, Olcese U, Hanlon EC, Nir Y, Cirelli C, Tononi G. Local sleep in awake rats. Nature. 2011 Apr 28;472(7344):443-7. doi: 10.1038/nature10009. PMID: 21525926; PMCID: PMC3085007.

[46] Isomura Y, Sirota A, Ozen S, Montgomery S, Mizuseki K, Henze DA, Buzsáki G. Integration and segregation of activity in entorhinal-hippocampal subregions by neocortical slow oscillations. Neuron. 2006 Dec 7;52(5):871-82. doi: 10.1016/j.neuron.2006.10.023. PMID: 17145507.

[47] Levenstein, D., Buzsáki, G., Rinzel J. NREM sleep in the rodent neocortex and hippocampus reflects excitable dynamics. *Nat Commun.* 10(1):2478. (2019)

[48] Lendner JD, Helfrich RF, Mander BA, Romundstad L, Lin JJ, Walker MP, Larsson PG, Knight RT. An electrophysiological marker of arousal level in humans. Elife. 2020 Jul 28;9:e55092. doi: 10.7554/eLife.55092. PMID: 32720644; PMCID: PMC7394547.

[49] Colombo MA, Napolitani M, Boly M, Gosseries O, Casarotto S, Rosanova M, Brichant JF, Boveroux P, Rex S, Laureys S, Massimini M, Chieregato A, Sarasso S. The spectral exponent of the resting EEG indexes the presence of consciousness during unresponsiveness induced by propofol, xenon, and ketamine. Neuroimage. 2019 Apr 1;189:631-644. doi: 10.1016/j.neuroimage.2019.01.024. Epub 2019 Jan 11. PMID: 30639334.

[50] Funk CM, Peelman K, Bellesi M, Marshall W, Cirelli C, Tononi G. Role of Somatostatin-Positive Cortical Interneurons in the Generation of Sleep Slow Waves. J Neurosci. 2017 Sep 20;37(38):9132-9148. doi: 10.1523/JNEUROSCI.1303-17.2017. Epub 2017 Aug 16. Erratum in: J Neurosci. 2017 Nov 1;37(44):10770. PMID: 28821651; PMCID: PMC5607463.

[51] Watson BO, Levenstein D, Greene JP, Gelinas JN, Buzsáki G. Network Homeostasis and State Dynamics of Neocortical Sleep. Neuron. 2016 May 18;90(4):839-52. doi: 10.1016/j.neuron.2016.03.036. Epub 2016 Apr 28. PMID: 27133462; PMCID: PMC4873379.

[52] Grosmark AD, Buzsáki G. Diversity in neural firing dynamics supports both rigid and learned hippocampal sequences. Science. 2016 Mar 25;351(6280):1440-3. doi: 10.1126/science.aad1935. PMID: 27013730; PMCID: PMC4919122.

[53] Grosmark AD, Mizuseki K, Pastalkova E, Diba K, Buzsáki G. REM sleep reorganizes hippocampal excitability. Neuron. 2012 Sep 20;75(6):1001-7. doi: 10.1016/j.neuron.2012.08.015. PMID: 22998869; PMCID: PMC3608095.

[54] Eckman, JP, Oliffson Kamphorst, S and Ruelle, D. Recurrence Plots of Dynamical Systems. Europhysics Letter. Volume 4:9. (1987) https://doi.org/10.1209/0295-5075/4/9/004

[55] Pitsik E, Frolov N, Hauke Kraemer K, Grubov V, Maksimenko V, Kurths J, Hramov A. Motor execution reduces EEG signals complexity: Recurrence quantification analysis study. Chaos. 2020 Feb;30(2):023111. doi: 10.1063/1.5136246. PMID: 32113225.

[56] Bandt, C. & Pompe, B., Permutation Entropy: A Natural Complexity Measure for Time Series. *Phys. Rev. Lett.* **88**(17), 174102 (2002).

[57] Povysheva NV, Gonzalez-Burgos G, Zaitsev AV, et al. Properties of excitatory synaptic responses in fast-spiking interneurons and pyramidal cells from monkey and rat prefrontal cortex. Cereb Cortex. 2006;16(4):541-552. doi:10.1093/cercor/bhj002

[58] Shannon, C. E., A mathematical theory of communication (parts I and II), *Bell System Tech. J.* **27**, 379-423 (1948).

[59] Donoghue T, Haller M, Peterson EJ, Varma P, Sebastian P, Gao R, Noto T, Lara AH, Wallis JD, Knight RT, Shestyuk A, Voytek B. Parameterizing neural power spectra into periodic and aperiodic components. Nat Neurosci. 2020 Dec;23(12):1655-1665. doi: 10.1038/s41593-020-00744-x. Epub 2020 Nov 23. PMID: 33230329.

Supplementary Material

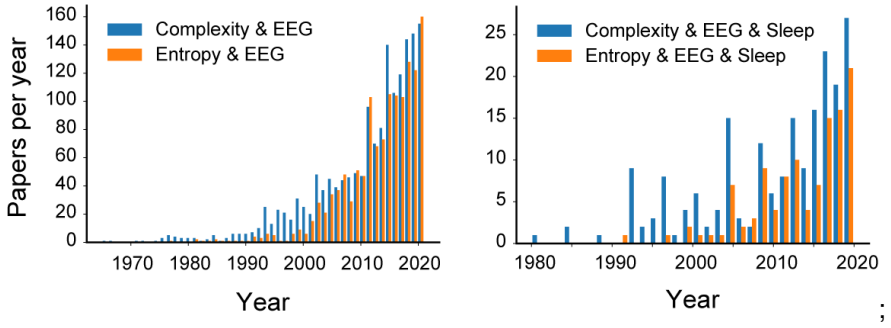

Figure S1: Complexity analysis is a growing framework to understand EEG dynamics. Left: Number of Pubmed papers published in the last 50 years containing the words (in their abstract or title): Complexity and EEG or Entropy and EEG. Right Number of Pubmed papers published containing the words: Complexity and EEG and Sleep, or Entropy and EEG and Sleep. Data comes from the Pubmed database (https://pubmed.ncbi.nlm.nih.gov)

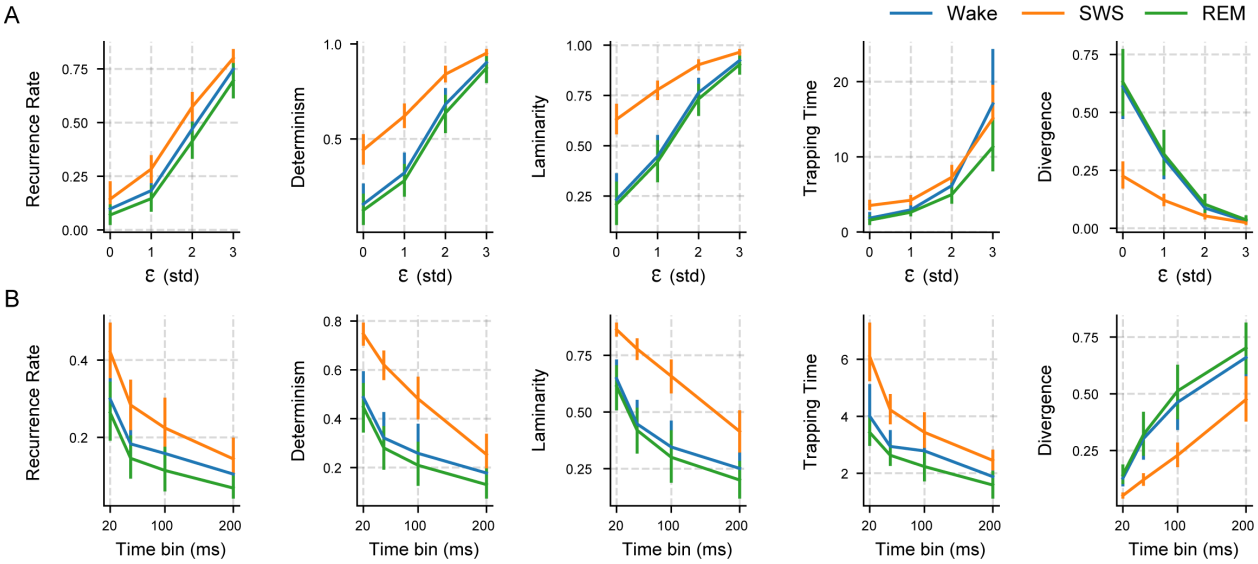

Figure S2: RQA is robust to parameter choice. **A** RQA metrics for different tolerance levels ϵ for defining recurrence in phase-space. We vary ϵ from 0 std to 4 std of the population firing counts. Setting ϵ to 0 means that a recurrence occurs between two times for the exact same neuronal firing pattern. The time bin is kept fix at 50*ms*. **B** RQA metrics for different time binning of the population activity. Time bins are changed from 20 ms to 200 ms in order to define the firing variable for each neuron. The ϵ is kept fix at 1 std. The mean and its corresponding 95 % confidence intervals are shown for each plot.

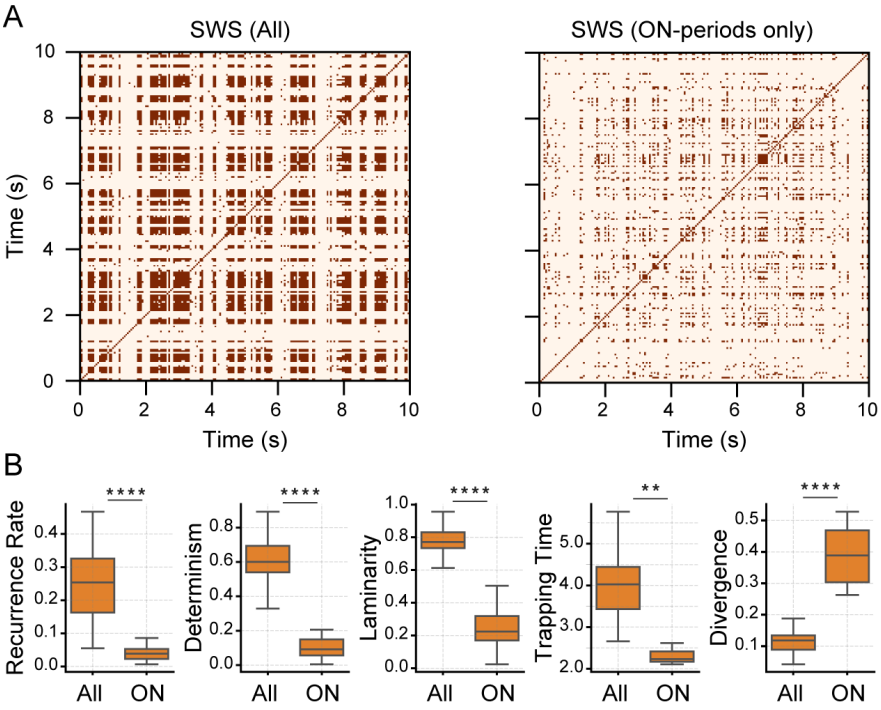

Figure S3: Recurrence analysis during the SWS ON-periods. **A** Recurrence plots constructed from 10 *s* intervals after binning the spike-trains in 50 *ms* windows. **B** Recurrence Quantification Analysis using 5 RQA metrics (titles in panels). For each metric, box-plots are constructed from the results of 12 animals and 24 sessions (outliers are not shown).NS: Non-significant ($P > 0.05$)

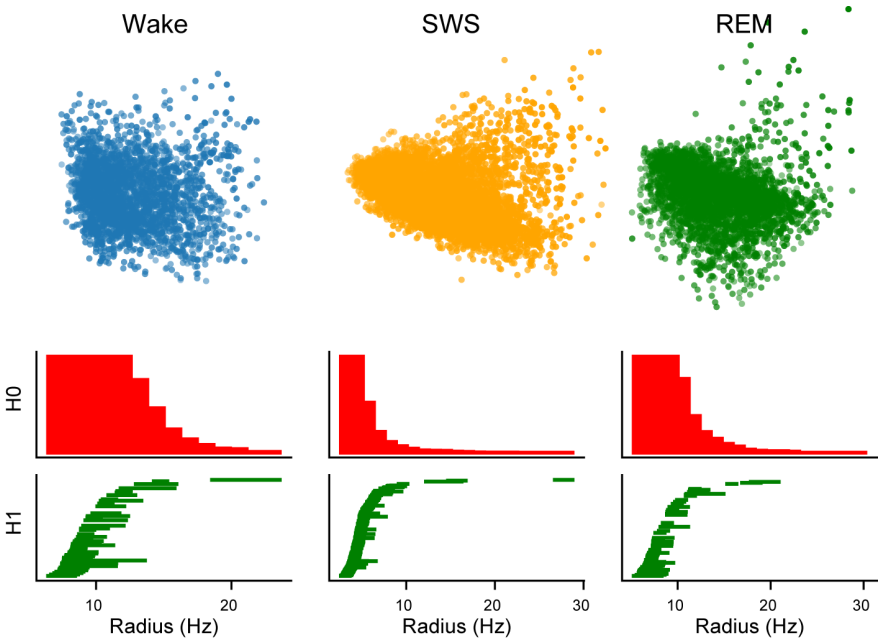

Figure S4: Persistent Homology during the sleep-wake states in the neocortex. Top panels: Point cloud obtained after dimensionality reduction. A representative animal is shown during Wake, SWS and REM sleep. Bottom panels: Betti 0 (HO) and Betti 1 (H1) barcodes for the same animal shown in the top panel. The length of each bar shows the level of persistence of each Betti 0 and 1 component.

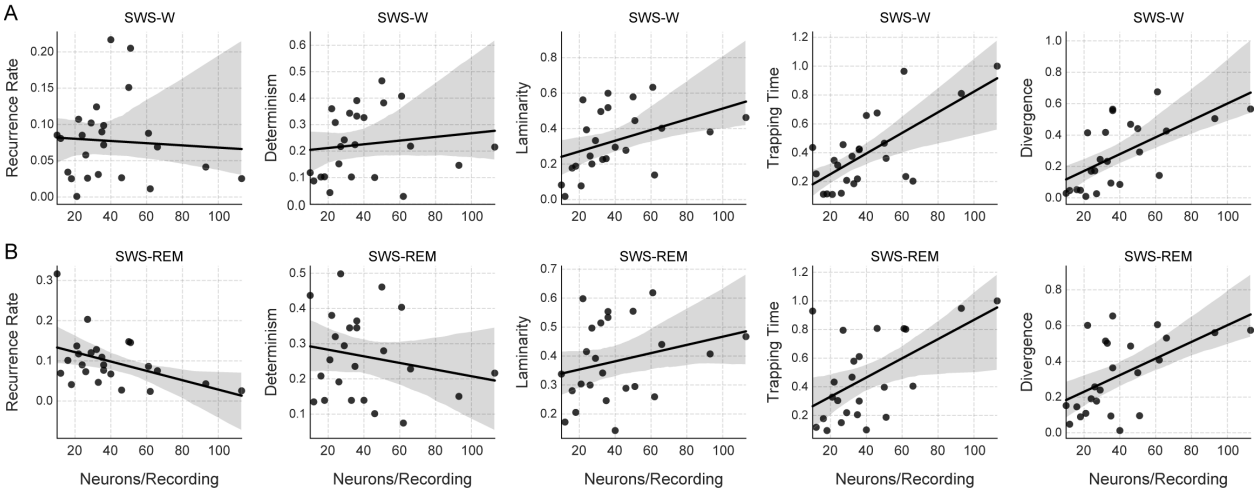

Figure S5: RQA differences between states correlate with the number of neurons recorded. Absolute RQA differences between states as a function of the number of simultaneously recorded neurons. Each dot shows a recording session while the solid line the linear regression estimate with its 95 % confidence interval. **A** shows the SWS-Wake difference, while **B** the SWS-REM difference.

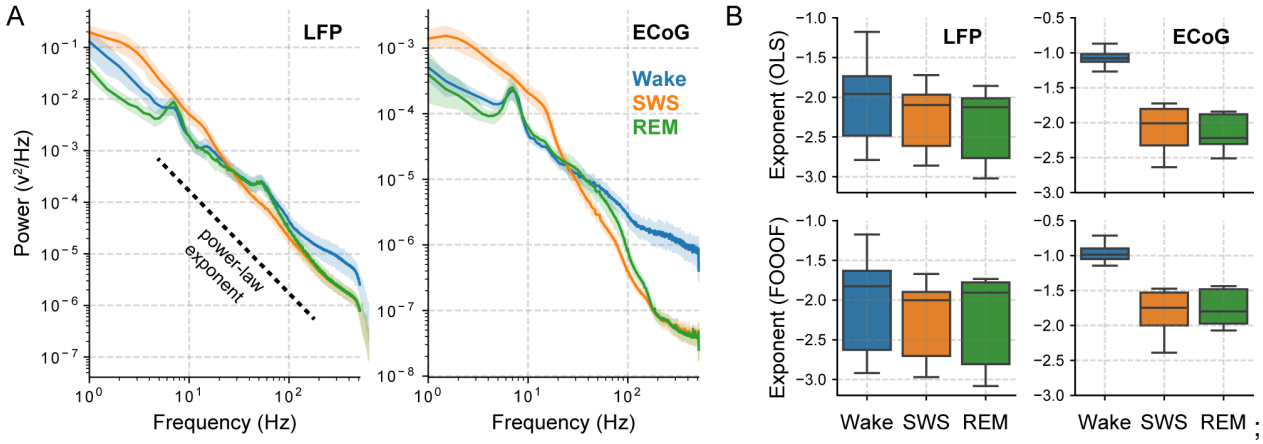

Figure S6: Power spectrum slope differs between states. **A** LFP [ECoG] recordings coming from the frontal cortex [M1 cortex] during the states of Wake, SWS and REM sleep. The mean and its corresponding 95 % confidence intervals are shown for each plot. **B** Power spectrum exponents calculated through ordinary least-squares fit on a log-log scale (OLS) or through the FOOOF parametrized spectra (FOOOF) [59] which only includes the aperiodic component.

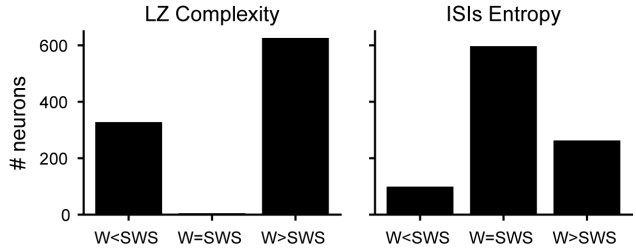

Figure S7: Single neurons deviate from the ensemble behaviour. Complexity of single neuron firing pattern between Wake and SWS. Each bar shows the total number of neurons whose temporal complexity decreased, remained equal or increased. 2 metrics are shown. Left: Lempel-ziv complexity of single neuron binary raster. Right: Inter-spike interval histogram entropy

Metric	W-SWS-REM	W-SWS		REM-SWS	
	P	P	Cohen's D	P	Cohen's D
RR	1.8×10^{-8}	4.6×10^{-4}	0.7	9.7×10^{-9}	1.0
DET	1.1×10^{-8}	7.9×10^{-5}	1.6	9.7×10^{-9}	2.0
LAM	3.3×10^{-9}	2.2×10^{-5}	1.7	4.0×10^{-9}	1.9
TT	1.8×10^{-8}	4.2×10^{-5}	1.2	2.3×10^{-8}	1.5
DIV	9.5×10^{-8}	7.9×10^{-5}	1.1	1.2×10^{-7}	1.2

Table S1: Statistical comparisons Fig 2C

Metric	W-SWS-REM	W-SWS		REM-SWS	
	P	P	Cohen's D	P	Cohen's D
RR	1.5×10^{-3}	1.8×10^{-2}	2.4	1.3×10^{-3}	1.6
DET	8.0×10^{-4}	3.6×10^{-2}	4.4	5.3×10^{-4}	3.2
LAM	8.0×10^{-4}	3.6×10^{-2}	5.2	5.3×10^{-4}	3.5
TT	8.0×10^{-4}	3.6×10^{-2}	2.9	3.5×10^{-4}	2.5
DIV	1.5×10^{-3}	1.8×10^{-2}	2.9	1.3×10^{-3}	2.4

Table S2: Statistical comparisons Fig 3B

Metric	W-SWS-REM	W-SWS	REM-SWS
	P	P , Cohen's D	P, Cohen's D
Sample Entropy	6.2×10^{-7}	1.4×10^{-2}, 0.7	2.7×10^{-7}, 2.4
Permutation Entropy	4.1×10^{-9}	1.3×10^{-3}, 1.2	1.6×10^{-9}, 1.6
Lempel-Ziv Complexity	1.9×10^{-9}	4.2×10^{-5}, 3.3	1.6×10^{-9}, 3.6

Table S3: Statistical comparisons for the complexity metrics on real LFPs, shown in Fig 5D

Metric	W-SWS-REM	W-SWS	REM-SWS	SWS(All)-SWS(On)
	P	P , Cohen's D	P, Cohen's D	P, Cohen's D
Sample Entropy	2.6×10^{-7}	3.0×10^{-6}, 1.35	3.0×10^{-6}, 1.5	1.6×10^{-6}, 1.6
Permutation Entropy	2.2×10^{-7}	1.0×10^{-6}, 0.4	1.1×10^{-5}, 0.8	1.1×10^{-7}, 1.2
Lempel-Ziv Complexity	2.5×10^{-7}	6.0×10^{-6}, 0.76	3.0×10^{-6}, 1.9	1.2×10^{-7}, 2.0

Table S4: Statistical comparisons for the complexity metrics on synthetic LFPs, shown in Fig 5D,E